Tracers Applied in Radioguided Surgery

5

Anton Bunschoten, Nynke S. van den Berg, Renato A. Valdés Olmos, Jacobus A.K. Blokland, and Fijs W.B. van Leeuwen

Contents

A. Bunschoten • N.S. van den Berg
F.W.B. van Leeuwen (✉)
Interventional Molecular Imaging Laboratory, Department of Radiology, Leiden University Medical Center (LUMC), Leiden, The Netherlands
e-mail: f.w.b.van_leeuwen@lumc.nl

R.A. Valdés Olmos
Interventional Molecular Imaging Laboratory, Department of Radiology, Leiden University Medical Center (LUMC), Leiden, The Netherlands

Departments of Nuclear Medicine, Antoni van Leeuwenhoek Hospital - Netherlands Cancer Institute (AvL-NKI), Amsterdam, The Netherlands

J.A.K. Blokland
Nuclear Medicine, Department of Radiology, Leiden University Medical Center (LUMC), Leiden, The Netherlands

Abstract

Radioguided surgery (RGS) allows a surgeon to intraoperatively identify the lesions of interest. This technique relies on the accumulation of a radiotracer in the lesion(s) of interest. Such accumulation can occur via the local administration of the radiotracer, followed by local staining or passive drainage via the lymphatic system, or can occur via the systemic administration followed by retention or targeted accumulation of the radiotracer. The range of radiotracers applied in RGS varies from the radioactive isotope itself, to small molecules, peptides, antibodies, and colloids. The choice of the radionuclide depends on various factors, such as half-life, desired radiation type and energy, and (chemical) means to attach it to an active entity. An often overlooked factor is the radiation burden for the patient and the medical personnel. The introduction of optical imaging technologies, such as fluorescence and Cherenkov imaging, expands the utility of RGS.

5.1 Introduction

The concept of radioguided surgery (RGS) can provide the operating specialist with information regarding the location and margins of target lesions

K. Herrmann et al. (eds.), *Radioguided Surgery: Current Applications and Innovative Directions in Clinical Practice*, DOI 10.1007/978-3-319-26051-8_5

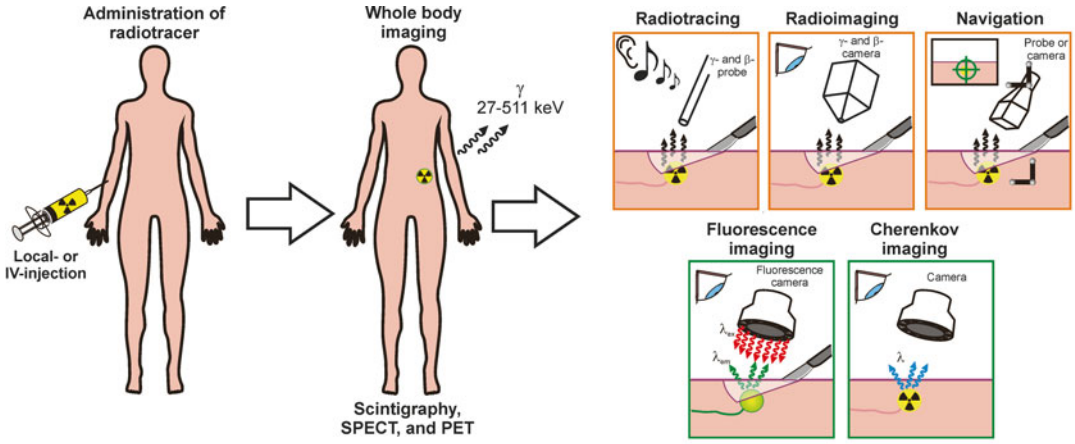

Fig. 5.1 Schematic representation of the possibilities with radio- and hybrid tracers

during surgery and as such can help improve the accuracy of the surgical procedure (Fig. 5.1). RGS requires two things: (1) the availability of a tracer emitting a nuclear signal (possibly accompanied by and optical signal) that accumulates at the site of interest and (2) (portable) detectors that can detect the tracers nuclear signal, thereby providing the surgeon with acoustic or visual feedback regarding its location. Fully integrated whole body preoperative (nuclear) imaging and intraoperative RGS using the same radiotracer (single injection) is the most superior way to perform RGS as it allows the nuclear medicine physician and surgeon to jointly generate a (virtual) roadmap regarding the location of the lesions, thereby also enabling the identification of unexpected lesions at distant locations (Fig. 5.1). During the intervention, radioguidance, possibly in combination with an optical component, can provide the surgeon with real-time information regarding the location of the lesions and helps confirm accurate lesion resection. In combination with state-of-the-art navigation equipment, the preoperative nuclear information can provide additional (virtual) intraoperative guidance to improve RGS (Fig. 5.1) [1]. The technical approach and the detectors required for RGS will be discussed in further chapters.

This chapter discusses the radio- and hybrid tracers applied in the field of RGS. Hereby we only focus on tracers that have been used in a clinical setting.

5.2 General Categories and Routes of Administration for Radiotracers

The radiotracers applied in RGS can roughly be divided into four general categories: (1) radiocolloids (Fig. 5.2), (2) small molecules (Fig. 5.3), (3) peptides (Fig. 5.4), and (4) antibodies and antibody fragments (Fig. 5.5). Radiotracers can be administered locally, e.g., when using a radiocolloid for sentinel lymph node (SLN) biopsy, or intravenously, e.g., when using targeted antibodies.

5.2.1 Local Administration

The most widespread application of RGS is the SLN biopsy procedure. For this application, radiolabeled colloid particles (Fig. 5.2) are injected into or directly surrounding the primary tumor, from which they drain via the local lymphatic pathways to the SLN(s). These lymph nodes can then be removed via RGS to be examined at pathology for the presence of metastases. Although the mechanism may differ, upon reaching the SLN(s), these radiocolloids become entrapped via interaction with macrophages and histiocytes lining the sinuses of the nodes [2]. In SLN identification applications, movement of the tracer to the SLN is a physical phenomenon driven by lymphatic flow. Hence, when the

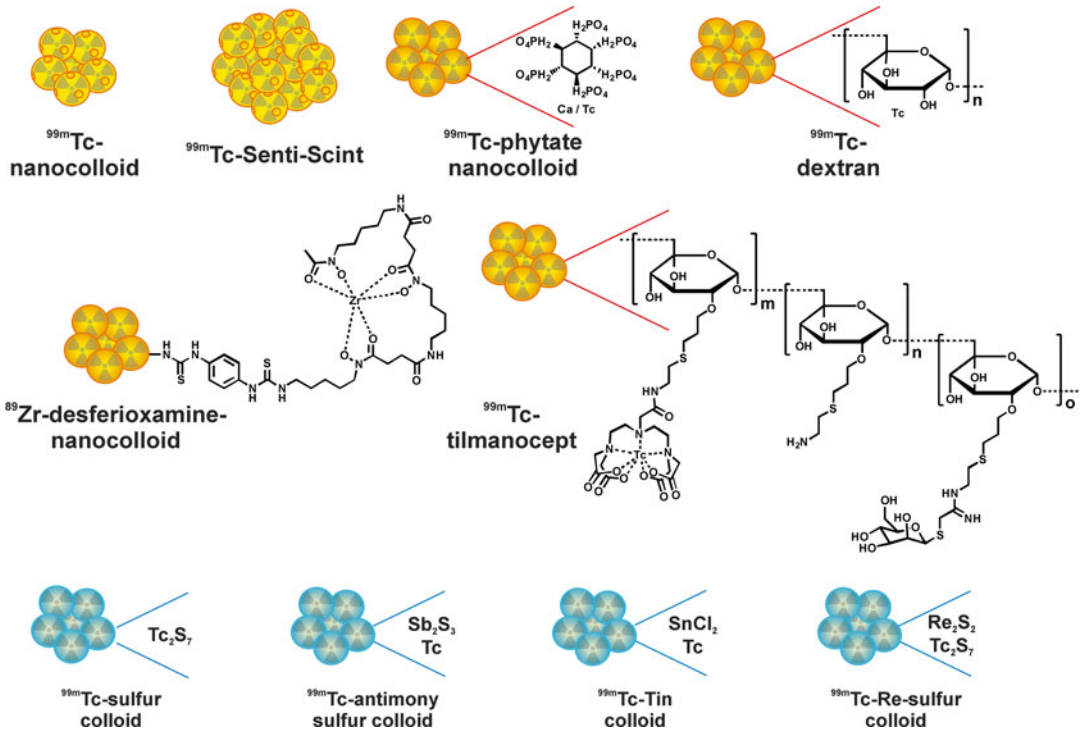

Fig. 5.2 Radiocolloids applied in RGS

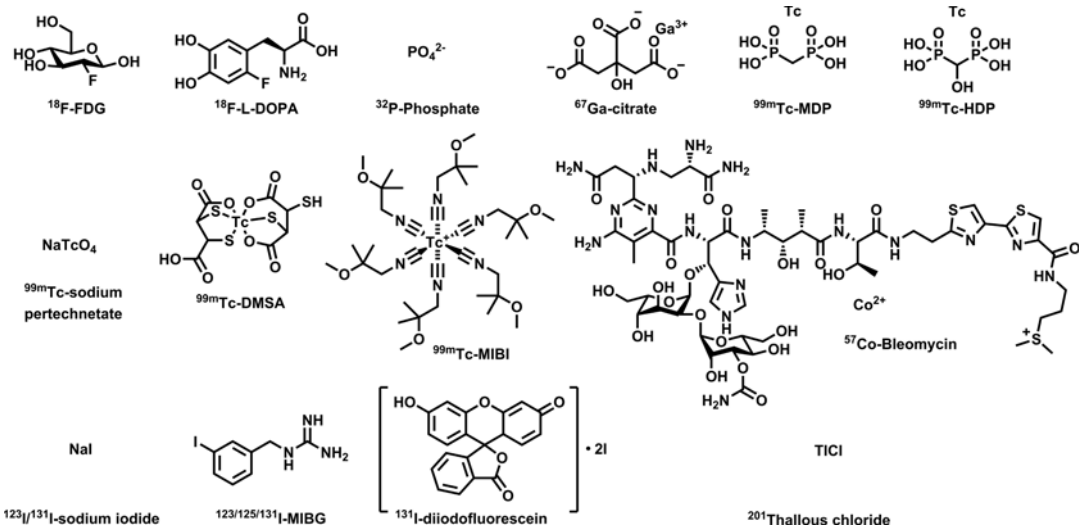

Fig. 5.3 Small-molecule radiotracers applied in RGS

lymphatic flow is abundant, e.g., following the injection of a large volume of tracer, saturation of the SLN can occur, leading to overflow into higher-echelon nodes. This effect is similar to pouring a bottle of champagne on a pyramid of champagne glasses. Initially only the first glass will fill up, but when more champagne is added, eventually all glasses will fill up. However, when

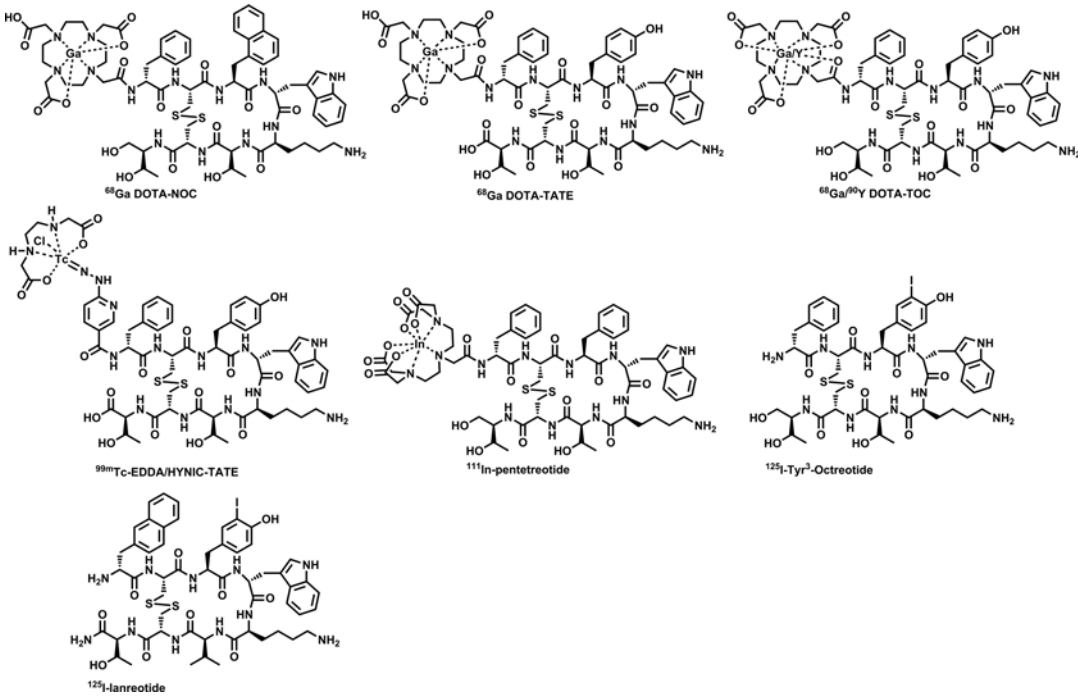

Fig. 5.4 Peptide-based radiotracers applied in RGS

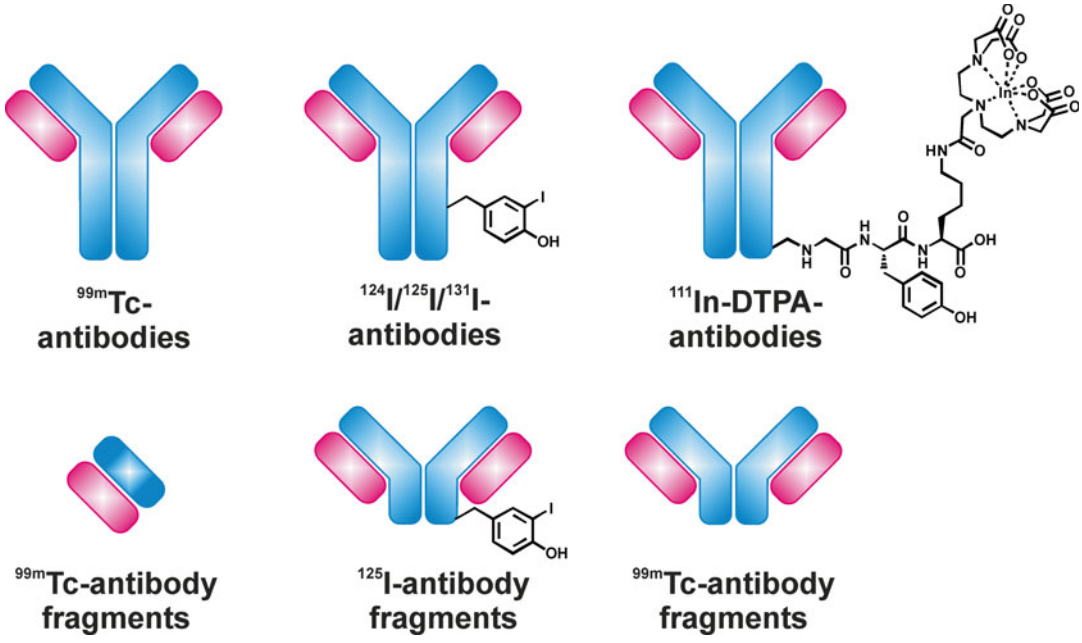

Fig. 5.5 Radiolabeled antibodies and antibody fragments applied in RIGS

the injected volume is limited and the SLN procedure is combined with dynamic imaging, retention of radiocolloid allows for accurate identification of the SLN(s).

For the radioguidance toward the sentinel lymph node in SLN biopsies in various cancer types, ^{99m}Tc-labeled radiocolloids are widely applied (Fig. 5.2). Radiocolloid labeling occurs via the complexation of ^{99m}Tc via various donor atoms in the colloids. The size of the colloidal particles is probably the most important variable and determines the tracer dynamics. Particles with a diameter above 500 nm show very limited drainage via the lymphatic system [3]. On the other side, particles between 5 and 12 nm can penetrate the capillary membranes and rapidly migrate through the lymphatic system and thus require targeting mechanisms using, e.g., mannose to be retained in the SLN [4–6]. Obviously here the chance of overflow to higher-echelon nodes is greatest. Medium-sized colloidal particles ranging between 10 and 200 nm are reported to show the best balance between drainage kinetics via the lymphatics and retention in the SLN(s) [2, 7]. An overview of the different SLN tracers and their sizes has been provided by van den Berg et al. [8].

A local injection, guided by ultrasound or X-ray imaging, with, e.g., (large) ^{99m}Tc-labeled colloidal particles, can also be used to mark nonpalpable (breast) tumors, essentially providing temporary radioactivity–based tattoos. This approach was shown a valid alternative to wire-guided localization (WGL), in which a hooked wire is placed preoperatively to locate the tumor during surgery [9]. The procedure that applies radioactive signatures of a radiocolloid to intraoperatively excise the tumors under RGS is called radioguided occult lesion localization (ROLL) [10]. A similar procedure, where a radioactive titanium seed is placed to locate the tumor, is called radioguided seed localization (RSL). If this procedure is performed with a radiolabeled colloidal particle that also drains to the SLN(s), ROLL can be combined with a SLN biopsy procedure, which has been named sentinel node and occult lesion localization (SNOLL) [10, 11].

5.2.2 Intravenous Administration

The class of small molecule-based radiotracers is the oldest and most diverse class of tracer used in medicine. It consists of radiolabeled molecules mimicking hormones, such as metaiodobenzylguanidine (MIBG) [12]; amino acids, such as 3,4-dihydroxyphenylalanine (DOPA) [13], glucose, such as fluorodeoxyglucose (FDG) [14]; and mimicking building blocks, such as bisphosphonates (Fig. 5.3) [15]. In general these tracers are widely available and/or easy to prepare locally. After distribution through the patients' venous system, these tracers show increased uptake in diseased areas based on the increased metabolism and/or increased proliferation of malignant cells in comparison to healthy tissue.

Although somewhat larger than the small molecules, the relatively small size of receptor targeting peptides (Fig. 5.4) means that they have favorable kinetics. Since they can be produced synthetically, this class of compounds is relatively cheap compared to, e.g., antibodies. Moreover, the variety in which peptide sequences can be produced, and thus the variety of receptors that can potentially be targeted using such compounds, is endless.

To introduce a radionuclide in peptide tracers, in most tracers a bifunctional linker is introduced (Fig. 5.4). Such a bifunctional linker consists of donor atoms or groups that can form a complex with the radionuclide and a reactive group to allow conjugation to the targeting peptide. The introduction of the isotope can be performed just before applying the radiotracer. Generally receptor targeted peptides are injected intravenously to allow distribution via the blood circulation and finally targeting of a disease specific receptor.

In radioimmunoguided surgery (RIGS), radiolabeled antibodies or antibody fragments (Fig. 5.5) are used to target receptor molecules expressed on the lesion(s) of interest. Such antibodies are raised against a specific biomarker that is overexpressed in certain malignancies. The advantages of using an antibody as targeting moiety are their high specificity, affinity, and avidity for the biomarker it has been raised against. Conversely, nonspecific

uptake in organs such as the liver and spleen may increase the radiation burden for the patient. At the same time, long circulation times of antibodies demand a long time interval between administration and imaging and/or RIGS. This interval can vary significantly from 2 to 24 days to allow sufficient clearance of unbound antibodies [16–18]. Several options are available to deal with the circulation times: (1) use of isotopes with a long half-life such as ^{89}Zr, ^{111}In, or ^{125}I, to ensure the presence of a radioactive signal after multiple days; (2) pre-targeting, which is the use of a reactive or bivalent antibody, followed after a couple of days with the (reactive) radioisotope [19, 20]; and (3) use antibody fragments that show an increased clearance rate [21]. To introduce a radionuclide in the antibodies, three options are available. Either the radionuclide is complexed by donor atoms of the antibody itself (e.g., ^{99m}Tc) via covalent conjugation to amino acids in the antibody (e.g., ^{125}I) or via the before mentioned bifunctional linkers (e.g., ^{111}In) (Fig. 5.5).

To accommodate an additional optical signal, any one of the above tracer types may be converted into hybrid entities that include dyes [22]. Alternatively, the generation of Cherenkov light by beta-emitting isotopes can also enable optical guidance [23].

5.3 Radionuclides

Numerous radionuclides are available, or can be produced, for applications in nuclear imaging, RGS, radiotherapy, or combinations hereof. The choice for the (ideal) radionuclide is based on the availability of the radionuclide and the application for which it will be used. Ideally, a balance between the clinical demands (e.g., half-life, radiation type, radiation energy) and the ability to (chemically) attach the radionuclide to the tracer is found. Table 5.1 contains the physical characteristics of the radionuclides applied in RGS to date.

Table 5.1 Characteristics of radionuclides clinically applied for RGS

Radioisotope	Half-life	Radiation	Energy	Example of use during RGS
^{18}F	110 min	β^+	634 keV	Desai et al. [14]
^{32}P	14.3 days	β^-	690 keV	Selverstone et al. [24]
^{57}Co	271.8 days	β^-	14 keV	Woolfenden et al. [25]
		γ	122, 136 keV	
^{67}Ga	3.26 days	β^-	84 keV	Schattner et al. [26]
		γ	93, 184, 300 keV	
^{68}Ga	67.7 min	β^+	1.90 MeV	Kaemmerer et al. [27]
^{89}Zr	78.4 h	β^+	389 keV	Heuveling et al. [28]
		γ	909 keV	
^{90}Y	64 h	β^-	2.3 MeV	Collamati et al.[29]
^{99m}Tc	6.0 h	γ	141 keV	Gommans et al.[30]
^{111}In	2.80 days	γ	171, 245 keV	Panareo et al.[31]
^{123}I	13.2 h	β^-	23, 127 keV	Gallowitsch et al.[32]
		γ	27, 31, 159 keV	
^{124}I	4.18 days	β^+	1.5, 2.1 MeV	Strong et al. [33]
		γ	603, 1.69 MeV	
^{125}I	60.1 days	γ	27, 35 keV	Hinkle et al. [34]
^{131}I	8.02 days	β^-	606 keV	Jager et al. [35]
		γ	364 keV	
^{201}Tl	73 h	γ	71, 167 keV	Ubhi et al. [36]

Emissions >10 keV and abundance >5 % are included

For the selection of an isotope, radiation exposure of the patient and the medical personnel is also a major factor that needs to be taken into account. Not only is it necessary that the (long-term) benefits for the patient outweigh the possible side effects of radiation exposure, the dose received by the surgical staff during the intervention may also limit the amount of procedures that they can perform on a yearly basis. Table 5.2 contains the range of radiation doses both patients and medical personnel receive upon a RGS procedure with a certain radionuclide. Although this table shows the upper limits and possibly overestimates the dose, it clearly illustrates the differences between various radionuclides.

The patient dose clearly increases upon increased gamma-radiation energy (0.94 mSv for 100 MBq ^{99m}Tc compared to 8.1 mSv for ^{111}In) or by applying β-particle emitting isotopes (7.0 mSv for 370 MBq ^{18}F and 13 Sv for 550 MBq ^{131}I). The patient dose is generally justified by the benefits the patient obtains from accurate imaging,

Table 5.2 Radiation exposure of patient, surgeon, and non-nuclear personnel

Radionuclide	Injected dose per procedure (MBq (Farmacon))	Effective dose per patient (mSv)	RGS time postinjection (h)	Effective dose personnel (μSv h^{-1} (vh postinjection))	Max. 20 mSv yearly dose (h years^{-1})	Max. 5 mSv yearly dose (h years^{-1})	Max. 1 mSv yearly dose (h years^{-1})
^{18}F	370 (FDG)	7.0	1	35.0	571	143	29
			6	5.3	3779	945	189
	700 (FDG)	13.3	1	66.3	302	75	15
			6	10.0	1998	499	100
^{32}P	–	–	–	–	–	–	–
^{57}Co	37 (cyanocobalamin)	77.7	24	2.3	8696	2174	435
^{67}Ga	150 (citrate)	15	6	3.7	5357	1339	268
^{68}Ga	180	–	2	6.3	3175	794	159
^{89}Zr	37 (mAb)	22.2	72	3.4	5897	1474	295
^{90}Y	200 (mAb)	–	12	12.3	1627	407	81
^{99m}Tc	100 (nanocolloid)	0.94	1	1.9	10,335	2584	517
			24	0.14	147,322	36,830	7366
	700 (nanocolloid)	6.6	1	13.6	1476	369	74
			24	0.95	21,046	5261	1052
^{111}In	150 (pentetreotide)	8.1	24	10.1	1973	493	99
			48	7.9	2527	632	126
^{123}I	100 (MIBG)	1.3	4	3.6	5506	1377	275
			24	1.3	15,738	3935	787
^{124}I	180 (mAb)	–	168	9.6	2094	523	105
^{125}I	7 (albumin)	1.5	48	0.2	86,039	21,510	4302
^{131}I	100 (MIBG)	14	2	6.5	3058	764	153
	550 (sodium iodide)	13.10^{3}	24	33.2	602	150	30
	4000 (sodium iodide)	96.10^{3}	120	171	117	29	6
^{201}Tl	70 (TlCl)	15.4	1	1.2	16,101	4025	805

for the calculation, an average dose based on literature procedures was used. Data for the effective dose (mSv.MBq^{-1}) and for the effective dose rate (μSv.m^2.(h.MBq)$^{-1}$ were obtained from literature
The physical half-life was taken into account, not the biological half-life. Personnel were estimated to be on 1 m of the patient on average, and 1 m^2 of the personnel was exposed to the source

radiation therapy (e.g., ^{131}I), and/or RGS. Nevertheless, the choice for the radionuclide should be made carefully. For instance, the choice for applying ^{89}Zr results in a considerable radiation dose (22.2 mSv for 37 MBq ^{89}Zr). Radionuclides emitting β^--particles only show a high radiation burden for the patient, because this radiation has a very limited penetration. Radionuclides emitting β^+-particles and gamma-emission also generate a radiation burden for the medical personnel.

The radiation dose received by the medical personnel, e.g., the surgeon and the OR personnel, upon RGS, also deserves careful consideration. In contrast to the justification for the patient, medical personnel has no obvious benefit from the chosen procedure or radionuclide used during the procedure except for achieving an accurate resection. Nevertheless during the, generally long, surgical procedures (multiple hours), they stand in close proximity to the patient and expose themselves to the tracer-based radiation. Based on the level of training, medical personnel is allowed to be exposed to certain levels of radiation, generally divided in maximum exposures of 20, 5, and 1 mSv per year; general surgeons and OR personnel belong to the last group. Because these values represent the upper limits of radiation exposure that is legally allowed, this may influence the amount of procedures that can be performed on a yearly basis. For example, RGS with ^{18}F (370 MBq at 1 h postinjection) results in 35 μSv. h^{-1}. This means that personnel not trained in radiation hygiene can only be present at the operation table for 29 h a year (Table 5.2). An average operation to remove malignant lesions takes 4 h, which means that this person can only perform/attend seven procedures a year. A similar procedure with ^{99m}Tc (100 MBq at 1 h postinjection) allows untrained personnel to attend 129 4-h procedures per year (Table 5.2). An important factor in these calculations is the half-life of the isotope used and the time between injection and the RGS procedure. When the accumulation of the radiotracer allows a longer time between injection and RGS, a large reduction in the radiation exposure for medical personnel can be obtained (Table 5.2). This said, often a strong signal is required during surgery to allow for RGS.

5.3.1 Gamma-Radiation

The workhorses of nuclear medicine, and in particular RGS, are radionuclides that emit γ-photons (Fig. 5.6). Gamma-emitting radionuclides allow whole body imaging using planar scintigraphy and/or single-photon emission tomography (SPECT). Especially isotopes that emit low-to-medium energy (27–245 KeV) photons, such as ^{99m}Tc, ^{111}In, and ^{125}I, have been widely used for RGS. Reasons for their popularity are: (1) availability, (2) compatibility with clinically available gamma detectors, (3) well-developed (chemical) procedures for introducing these nuclides into radiotracers, and (4) energy-dependent tissue attenuation. A high-energy γ-emitter has a higher tissue penetration, improving the accuracy of preoperative imaging, but also results in a higher chance of background signals during RGS. Furthermore, high-energy γ-emissions demand a thickly shielded detector to improve the spatial resolution. The combination of low-to-medium energy photon emission with a short-to-medium half-life of the radionuclide results in a limited radiation burden for both the patient and medical personnel.

5.3.1.1 99m-Technetium

By far the most widely applied and available radioisotope is ^{99m}Tc. ^{99m}Tc has a half-life of 6 h and emits γ-photons of 141 keV, which is in the ideal range (100–200 KeV) for γ-detection by commercially available detectors. Due to this medium energy γ-radiation, the radiation burden for both patient and medical personnel is relatively low (Table 5.2). Pertechnetate ($^{99m}TcO_4^-$) can be collected from ^{99}Mo/^{99m}Tc generators by elution with saline and there is a range of possibilities for conjugation of this isotope to generate the desired radiotracers [37, 38]. Labeling of most ^{99m}Tc-based radiotracers is

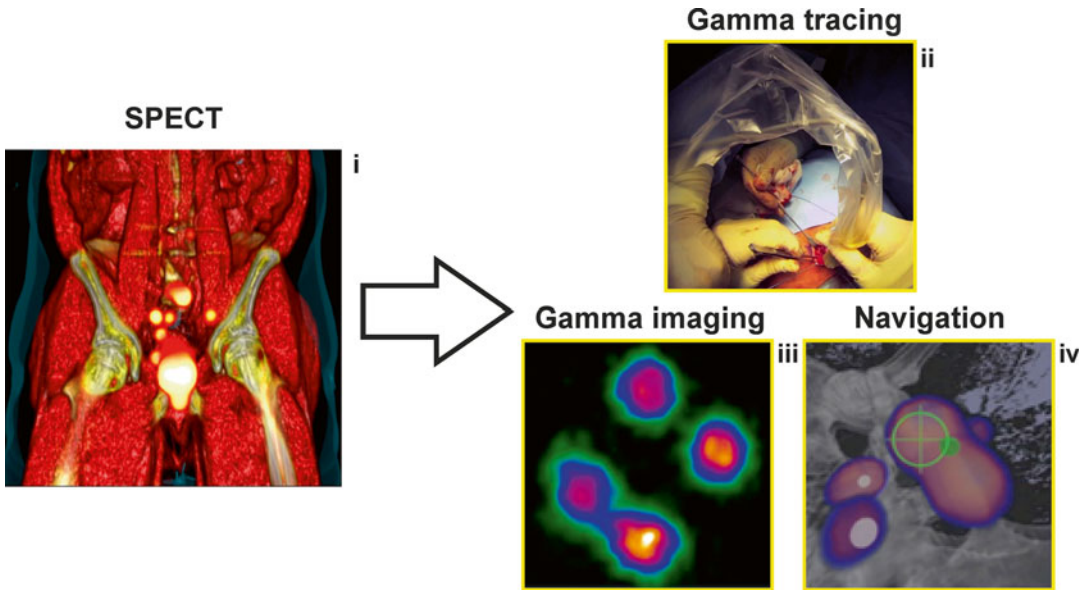

Fig. 5.6 Application of γ-emitters in RGS. (*i*) Whole body nuclear imaging by SPECT; (*ii*) intraoperative gamma tracing with acoustic gamma probe; (*iii*) intraoperative gamma imaging with gamma camera; (*iv*) virtual navigation based on preoperative SPECT imaging or intraoperative freehand γ-detection

performed by reducing the pertechnetate obtained from the generator with Sn(II)-based reducing agents in the presence of the coordinating agent of choice. Technetium can be stabilized through coordination to several donor atoms, e.g., N, O, P, S, and As [38]. Direct metal coordination can be achieved by small molecules that form the radiotracer together with ^{99m}Tc (such as hexakis-2-methoxy-2-methyl-isonitrile complex (MIBI) (Fig. 5.3)) [39], or it can be the functional part of a peptide, protein, or inorganic tracer itself (such as ^{99m}Tc-UBI$_{29–41}$ [40], ^{99m}Tc-nanocolloid, and ^{99m}Tc-sulfur colloid (Fig. 5.2) [30, 41]). Other than direct metal coordination, metal coordination can also occur through bifunctional chelates, for example, by applying hydrazinonicotinic acid (HYNIC) and diethylene triamine pentaacetic acid (DTPA) [42, 43].

Numerous materials have been applied to form radiocolloids for local injection, resulting in a large size range. Several inorganic particles are clinically applied for SLN biopsy and SNOLL applications such as ^{99m}Tc-sulfur colloid (15–5000 nm unfiltered or 15–400 nm filtered) [7, 11, 44, 45] (the United States) and ^{99m}Tc-antimony trisulfide (3–30 nm) [7, 45, 46] (Australia and Canada) (Fig. 5.7). ^{99m}Tc–tin colloids have also been applied, mainly in Japan. Their size can be controlled by the concentration of stannous chloride and ^{99m}Tc, resulting in particles of 50–1500 nm (Fig. 5.7) [45]. In some cases, like with ^{99m}Tc-rhenium sulfide (NanoCis) (20–100 nm), the stability and the formation of micro aggregates have limited use of the tracer [7, 46, 47]. Also organic-based colloid particles are applied for radioguided SLN biopsies. ^{99m}Tc-phytate particles (Fig. 5.2) are formed by the interaction of stannous phytate with Ca^{2+} present in serum. The size of these particles depends on the calcium concentration and in vitro experiments showed a size range of 150–1500 nm [45]. In Europe, ^{99m}Tc-labeled human serum albumin (HSA)-based colloids are most widely used for SLN biopsy procedures. HSA-nanocolloid (Nanocoll; mean diameter 20 nm; range 10–100 nm, Fig. 5.2) has shown to provide a superior retention in the SLN compared to radiolabeled HSA (vasculosis; mean

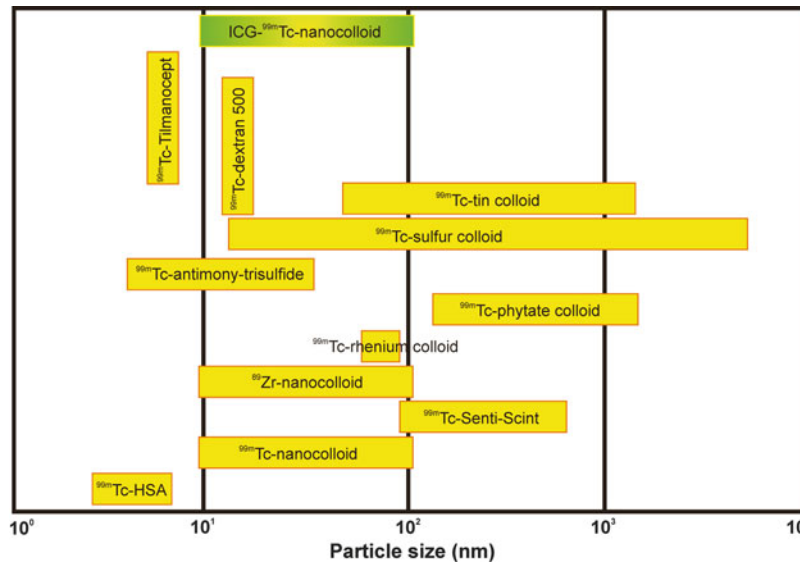

Fig. 5.7 Various size ranges of radiocolloids applied in RGS

diameter 7 nm) and is therefore widely applied [6, 30]. Next to the SLN biopsy, Nanocoll is also often used for ROLL and SNOLL procedures [48], sometimes in combination with large ^{99m}Tc-labeled albumin aggregates (e.g., ^{99m}Tc-MAA (10–90 μm) for-tumor demarcation [10]. Even the larger HSA-nanocolloid (SentiScint; mean diameter 205 nm; range 100–600 nm; Fig. 5.2) has shown promising results during SLN procedures [49, 50]. ^{99m}Tc-labeled dextran-based nanoparticles (14 nm) have been used for lymphatic mapping in, e.g., colon and breast cancer [51, 52]. A small dextran-based colloid (7 nm) with DTPA and mannose moieties conjugated to its structure has been developed for SLN mapping (Tilmanocept) (Fig. 5.2) [53–55]. This tracer is claimed to show faster clearance from the injection site and to have a stronger interaction with phagocytes [42].

Next to local administration, ^{99m}Tc-labeled compounds can also be administered intravenously. The most simple form herein is the ability of "free" ^{99m}Tc-pertechnetate to accumulate in the thyroid, due to its resemblance to iodine. Next to thyroid scintigraphy to evaluate for hot/cold nodules, pertechnetate can also be used for radioguidance during thyroidectomy [56].

Conjugated to six methoxyisobutylisonitrile ligands, ^{99m}Tc forms the hydrophobic and positively charged ^{99m}Tc-sestamibi (Fig. 5.3), which is rapidly taken up by mitochondria in (hyper)active cells. Next to its common application in cardiac imaging [57], ^{99m}Tc-sestamibi was also shown to allow the evaluation of tumor margins in patients with breast cancer showing promising results for the detection of small foci [58]. Furthermore, the normal distribution of ^{99m}Tc-sestamibi was evaluated in 5 volunteers followed by the RGS of one patient suspected of a brain tumor. ^{99m}Tc-sestamibi-based RGS resulted in the accurate detection and removal of the brain lesions diagnosed as metastases of renal cell carcinoma [59]. Due to its uptake in (hyper)active cells, ^{99m}Tc-sestamibi has also been applied in the detection of abnormalities in the (para)thyroid [60–64].

^{99m}Tc-dimercaptosuccinic acid (DMSA) (Fig. 5.3) is believed to accumulate in tumors due to their acidic environment [65]. Therefore, ^{99m}Tc-DMSA has been applied for the detection of thyroid cancer. In a study it was compared in 25 patients to ^{111}In-pentetreotide (see below) [66]. Although better results were found for ^{99m}Tc-DMSA, it is no longer commercially available [67].

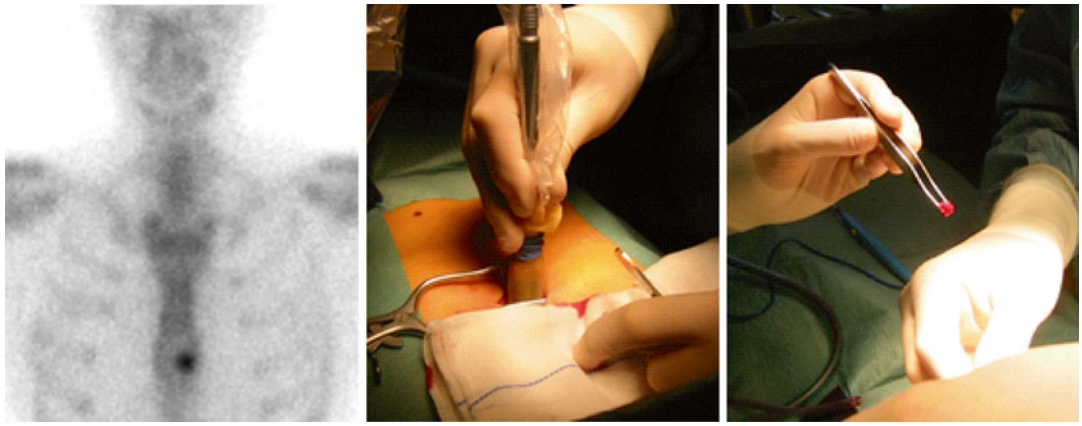

Fig. 5.8 Patient with a sternal metastasis, resected via ^{99m}Tc-MDP RGS

Bisphosphonates have a high affinity for hydroxyapatite, the mineral present in bones. Bisphosphonates especially tend to accumulate in sites of active bone formation, which occurs in bone lesions. Therefore, ^{99m}Tc-labeled bisphosphonates have been applied for radioguided biopsies and surgery of bone lesions. RGS based on ^{99m}Tc-medronic acid (MDP) and ^{99m}Tc-oxidronate (HDP) (Figs. 5.3 and 5.8) was shown to reduce the procedure time and to improve the localization of the lesions [15, 68–70].

Coordinated by HYNIC and ethylenediamine N,N'-diacetic acid (EDDA), ^{99m}Tc has also been conjugated to receptor targeting peptides such as the somatostatin analogue octreotate (Fig. 5.4). Upon intravenous administration, the peptide targets the somatostatin receptors, commonly overexpressed on neuroendocrine tumors. This radiotracer was used for RGS of four carcinoids and five pancreatic neuroendocrine tumors, resulting in accurate detection of the lesions and an increased detection of lymph node metastases [43].

^{99m}Tc has also been used to label antibodies, e.g., SM3 against polymorphic epithelial mucin and H17E2 against placental- and germ cell alkaline phosphatases; both are biomarkers that are overexpressed in ovarian cancer (Fig. 5.5). In 16 patients (1 patient for H17E2 and 15 patients for SM3), these labeled antibodies were shown to allow detection of ovarian cancer, both in vivo and in excised tissue specimens [71]. An ^{99m}Tc-labeled antibody fragment against carcinoembryonic antigen (CEA) (IMMU 4-Fab) (Fig. 5.5) was applied for RIGS in 65 patients with colorectal tumors resulting in more accurate diagnosis and in determining the extent of the lesion and possible lymph node intrusion [72]. ^{99m}Tc labeled anti-CEA antibody fragment F023C5 was unsuccessful in the detection of lesions in one lung cancer patient, but did show an increased uptake of radioactivity ex vivo [67, 73].

5.3.1.2 111-Indium

^{111}In is a γ-emitter with a half-life of 2.8 days. Similar to ^{99m}Tc, the photon energies of ^{111}In (171 and 245 keV) are in the optimum range for commercial gamma cameras. Due to the higher energy γ-radiation and the longer half-life, the radiation burden for patients and medical personnel is higher compared to ^{99m}Tc (Table 2). ^{111}In is produced by proton irradiation of ^{112}Cd and can be incorporated in radiotracers via bifunctional chelates such as DTPA and 1,4,7,10-tetraazacyclododecane-1,4,7,10-tetraacetic acid (DOTA), which can be chemically conjugated to targeting moieties such as a peptides, antibodies, and proteins.

For the RGS toward, e.g., neuroendocrine tumors, thyroid carcinomas, and meningiomas, ^{111}In-labeled somatostatin analogues are widely

applied (Fig. 5.4) [31, 66, 74–78]. The mechanism of tracer uptake is based on intravenous administration of the tracer, followed by specific binding to the somatostatin receptor. Panareo et al. reported that use of ^{111}In-DTPA-D-Phe^{1}-octreotide (^{111}In-pentetreotide) resulted in the excision of non-palpable neuroendocrine breast tumors that were not detected by conventional imaging techniques [31]. The use of a gamma probe in ^{111}In-DTPA-D-Phe^{1}-octreotide RGS towards midgut carcinoid and endocrine pancreatic tumors in 21 patients allowed detection of all tumor lesions >5 mm, while SPECT failed to detect lesions <9 mm [75].

Intravenous administration of ^{111}In-labeled anti-TAG72 (a tumor-associated glycoprotein) antibodies has been used for RIGS of colorectal carcinoma (37 patients) and ovarian cancer (5 patients). This resulted in the detection of several lesions that would have been missed by standard surgical exploration [79, 80]. RIGS towards prostate-specific membrane antigen (PSMA) using the antibody ^{111}In-capromab pendetide has been reported in one patient, which resulted in the excision of a tumor positive lymph node (Fig. 5.5) [81]. RIGS with ^{111}In has also been performed via a pretargeting approach [20]; in 13 patients with thyroid carcinoma, approximately 4 days after injection of a bivalent antibody directed against CEA and DTPA, ^{111}In-di-DTPA-tyrosyl-lysine was injected [82]. 3 ± 1 days after injection of the radiotracer, patients underwent RGS. Small lesions with a diameter below 0.3 cm could be detected successfully using this approach [19].

5.3.1.3 57-Cobalt

^{57}Co is mainly a γ-emitter that emits photons of 122 and 136 keV. This radionuclide has a long half-life of 271.8 days. Due to its long half-life and the emission of low-energy β^--particles, the radiation burden for the patient is high (Table 2). This radioisotope is produced by proton irradiation of natural iron and nickel. Bleomycin, a cytostatic, was labeled with ^{57}Co via complexation of the bivalent cobalt ion by the molecule itself. 21 lung cancer patients were injected intravenously with bleomycin (Fig. 5.3), which was labeled via complexation of the divalent ^{57}cobalt ion [83]. Bleomycin itself binds and damages DNA and is therefore most active against fast dividing cells, such as in malignant tissue. ^{57}Co-labeled bleomycin was shown to allow the detection of lung tumors that would otherwise be missed [25]. However, the long half-life of ^{57}Co prevented dissemination of this technology.

5.3.1.4 67-Gallium

^{67}Ga is a γ-emitter (93, 184, and 300 keV) with a half-life of 3.26 days. Due to its medium half-life, high γ-energy emission (300 keV), and β^--emission, the use of ^{67}Ga results in a considerable radiation burden for the patient (Table 5.2). ^{67}Ga is produced by the irradiation of ^{68}Zn by charged particles, e.g., protons. After production the gallium is coordinated with citric acid to form gallium citrate (Fig. 5.3), which in itself is administered as radiotracer. ^{67}Ga-citrate is often used as radiotracer to detect inflammatory lesions, based on the transchelation of the ^{67}Ga to lactoferrin and siderophores released by leukocytes and microorganisms located at the site of infection [84, 85]. ^{67}Ga citrate has also been reported by Schattner et al. in the RGS toward extranodal lymphoma in one patient, where accumulation in the lesion was most likely caused by necrotic tissue and inflammatory responses [26].

5.3.1.5 123-Iodine

^{123}I is mainly a γ-emitter that emits photons of 27, 31, and 159 keV. Also this radionuclide emits β^--particles of 23 and 127 keV. The isotope has a half-life of 13.2 h. Due to its short half-life, the radiation burden caused by using this isotope is relatively low, although it is higher than ^{99m}Tc (Table 5.2). ^{123}I is produced by proton irradiation of ^{124}Xe, resulting in ^{123}Xe that subsequently decays to ^{123}I. Radioiodination, with all isotopes of iodine, is mainly performed by electrophilic substitution, which requires the (in situ) generation of I^+ species. These species can be obtained by the generation of mixed halogen species. Examples of applied oxidizing reagents that can generate mixed radiohalogen species are chloramine-T, iodogen, and N-chlorosuccinimide [86]. Mixed radiohalogen species (XCl) readily react with activated aryl compounds, such as phenols,

resulting in mono- or disubstitution at positions ortho to the hydroxyl group. Proteins can be radioiodinated due to the presence of tyrosine residues, although also histidine, tryptophan, and cysteine are sensitive to radioiodination [86, 87]. Non-activated aryl compounds can be radioiodinated via isotopic exchange, in which a non-radioactive iodine isotope is exchanged for a radioactive isotope, or via the electrophilic substitution of a stannylated precursor [88, 89]. Finally also radioiodine-labeled prosthetic groups can be added to the targeting moiety via a selective reaction, for instance, via conjugation to amine reactive groups [86, 87].

^{123}I has been used for RGS of thyroid cancer, both as Na^{123}I and as ^{123}I-MIBG (Fig. 5.3) [32, 90]. Injection of Na^{123}I will result in the accumulation in hyperactive regions of the thyroid, while ^{123}I-MIBG will accumulate in adrenergic tissue such as thyroid tumors. Because ^{131}I (see below) is less expensive, better available, and also often used for therapy, this isotope often replaces ^{123}I in thyroid-related procedures [67]. ^{123}I-MIBG has been applied for RGS-based detection of neuroblastoma (41 procedures) [12, 91] and for the detection of neuroendocrine tumors (4 patients) [66, 92].

5.3.1.6 125-Iodine

^{125}I is a γ-emitter with a half-life of 60.1 days that emits low-energy photons (35 keV). The low-energy photon emissions makes this isotope less suitable for whole body imaging, but well suited for RGS due to its low background radiation. ^{125}I is produced by neutron irradiation of ^{124}Xe, which leads to ^{125}Xe that then decays to ^{125}I. The labeling chemistry for this isotope essentially is identical to that of ^{123}I.

For RGS using the sodium salt to detect thyroid malignancies, generally other iodine isotopes are applied. ^{125}I has been used for the labeling of MIBG (Fig. 5.3). In a direct comparison between ^{123}I-MIBG (36 cases) and ^{125}I-MIBG (30 cases) for RGS in neuroblastoma patients, ^{125}I-MIBG showed a higher specificity. This difference can be explained by the low-energy emission of ^{125}I, which resulted in a lower background signal from surrounding tissue [91, 93].

There are also examples where iodination was used in combination with targeting peptides. For example, the somatostatin analogue ^{125}I-Lanreotide was used in 13 patients with breast carcinoma resulting in accurate positive margin resection [94]. Furthermore it was applied in 2 patients with gastrinomas, which are gastrin-secreting tumors that also overexpress the somatostatin receptor [95]. A different somatostatin analogue, ^{125}I-Tyr^3-octreotide, was applied in 12 patients suspected of neuroendocrine tumors or gastrinomas showing promising results in tumor-specific accumulation and intraoperative detection (Fig. 5.4) [96].

The long half-life of ^{125}I makes it ideal for RIGS with complete antibodies (Fig. 5.5). Most clinical radioiodinated RIGS studies using ^{125}I have been performed with antibodies targeting the tumor-associated glycoprotein 72 (anti-TAG-72), e.g., primarily in colorectal cancer but also in gastric, pancreatic, ovarian, lung, prostate, and breast cancer. It started with the murine B72.3 antibody, followed by the second-generation antibodies: CC49 and the humanized HuCC49 (for an extensive review, see ref. [67]). Alternatively, A_5B_7 (52 patients) [97] and CL58 (29 patients), targeting the carcinoembryonic antigen (CEA), resulted in the detection of colorectal cancer lesions [98]. ^{125}I-labeled F(ab')$_2$ antibody fragments, containing both binding domains of a whole antibody without the Fc region, directed against CEA (F023C5) were explored for RIGS. In a small patient group, F023C5 was used to identify breast and colorectal cancer. However, due to a low tumor detection rate during RGS (40 %), the investigators advised the use of more specific antibodies [99, 100]. Antibodies against the tumor-associated antigen 17-1A (EpCAM) has been radiolabeled with ^{125}I and applied in multiple patients to assist in locating non-palpable colorectal tumors or aiding in determining the resection margins [101–103]. Wang et al. intravenously injected ^{125}I-labeled antibodies (3H11) against human gastric cancer cells in 35 patients and showed high specificity and accuracy in detecting the lesions [67, 104].

Although little chemistry is involved, a completely different application of ^{125}I can be found in ^{125}I-labeled titanium seeds [105–107]. In a

procedure called radioguided seed localization (RSL), these seeds are placed under ultrasound or X-ray guidance to mark non-palpable breast tumors. It can be considered an alternative to WGL and ROLL and is of particular interest for use in a neoadjuvant setting. The systemic treatment, applied in the neoadjuvant setting to reduce the tumor volume before surgery, demands a considerable time (several weeks) between tumor localization and the actual surgery. WGL and ROLL are not ideal as they require the insertion of a twisted marker before treatment and/or the injection of ^{99m}Tc-labeled colloids just before surgery. ^{125}I-labeled seeds require only one procedure to place them and they remain detectable after >30 weeks [108]. Studies evaluating RSL showed a reduction in reoperations due to positive tumor margins and an increased patient convenience compared to the WGL [9, 109]. In comparison with ROLL, RSL showed the same surgical outcome in breast-conserving surgery [108].

5.3.1.7 131-Iodine

^{131}I emits both γ- and β^--radiation of 364 and 606 keV, respectively, and has a half-life of 8 days. ^{131}I is produced by neutron irradiation of natural tellurium. The labeling chemistry for this isotope resembles that of ^{123}I. ^{131}I induces a large radiation burden for the patient, as a result of its β^--emission. This, in combination with the accumulation of sodium iodide in the thyroid, has led to the therapeutic use of this isotope against thyroid malignancies. Due to the γ-emission, the isotope can be used for RGS, but caution is necessary with respect to the exposure of the medical personnel due to the large dosages (>1 GBq) used for therapeutic applications.

One of the first RGS studies reported in the literature applied ^{131}I-labeled diiodofluorescein (Fig. 5.3) to locate brain tumors [110, 111]. Fluorescein was shown to distribute throughout the body, but was slower cleared form the malignant tissue, which resulted in a detectable signal from the tumor between 3 and 8 h postinjection [112]. This observation led to the development of radioiodinated fluorescein. In 340 patients suspected of a space-occupying brain lesion, the detection of diiodofluorescein by a Geiger-Müller tube had an accuracy of 95 % [111].

^{131}I is the most used isotope to treat abnormalities of the thyroid and RGS towards, thyroid cancer [113–115]. However, after iodine-based therapy, many recurrent thyroid cancers are iodine insensitive and therefore other tracers have to be used for imaging and RGS (such as ^{99m}Tc-MIBI and ^{99m}Tc-DMSA). For the detection of neuroendocrine tumors, the use of ^{131}I-MIBG (Fig. 5.3) was shown feasible [116]. However, hepatic clearance can result in high background signals overshadowing the lesion of interest, which limits the application of all iodine-labeled MIBG tracers for the detection of neuroendocrine tumors in the area of the adrenal gland [66].

^{131}I has also been used for labeling of antibodies and antibody fragments, which resulted in the accurate detection of small lesions and allowed the evaluation of the resection margins (Fig. 5.5) [16, 35, 117, 118]. However, due to its β^--emission and relatively high-energy γ-photons, ^{131}I has been replaced by other iodine isotopes, such as ^{125}I, for RIGS applications.

5.3.1.8 201-Thallium

^{201}Tl is a γ-emitter that emits photons of 71 and 167 keV. T and the isotope has a half-life of 73 h. ^{201}Tl causes a considerable radiation dose for the patient, although the exposure for the medical personnel is relatively low (Table 5.2).

The radionuclide is produced by proton irradiation of ^{203}Tl, which yields ^{201}Pb that then decays into ^{201}Tl. An intravenous injection of ^{201}Thallous chloride (TlCl; Fig. 5.3) has been used in one RGS case towards parathyroid adenoma [36]. Since ^{201}Tl showed an increased uptake in areas of high cellular density with increased regional blood flow, the authors claim it allowed removal of the tumor, which was not detected by visible inspection.

5.3.2 Positron Radiation

A prominent part of nuclear medicine, and radiochemistry, focuses on radionuclides that emit β^+-particles or positrons in combination with

positron emission tomography (PET). The emitted positrons travel a maximum of a couple of millimeters through human tissue before they reach thermal energies and annihilate with an electron [119]. This annihilation results in the emission of two high-energy photons of 511 keV, which travel in opposite direction from the point of annihilation (180 ± 0.25°). Compared to SPECT imaging, PET imaging has a higher sensitivity and spatial resolution in whole body imaging. Because of these advantages, and their abundant clinical use, positron emitters have also been explored for RGS (Fig. 5.9).

Unfortunately, the advantages that apply for whole body imaging cannot be directly translated to RGS. Accurate localization of high-energy photons requires extensive shielding of the detectors, which generally converts them into heavy (and relatively large) devices. An interesting alternative is the selective detection of the positrons themselves. Due to the very limited range of positrons in tissue (<2 mm), this may yield a superficial detection technique that could allow for the accurate delineation of tumor margins. The fact that it is not straightforward to detect β^+-particles over the background of high-energy photons is underlined by the fact that there are only few reports that describe the intraoperative use of a β^+-selective probe [33, 120].

5.3.2.1 18-Fluorine

The most widely used β^+-emitter is ^{18}F, which emits β^+-particles of 634 keV and has a half-life of 110 min. Although high-energy photons (511 keV) are generated by the annihilation of the β^+-particles, the effective dose for the patient is relatively low. However, the high-energy photons result in a relatively high radiation burden for the

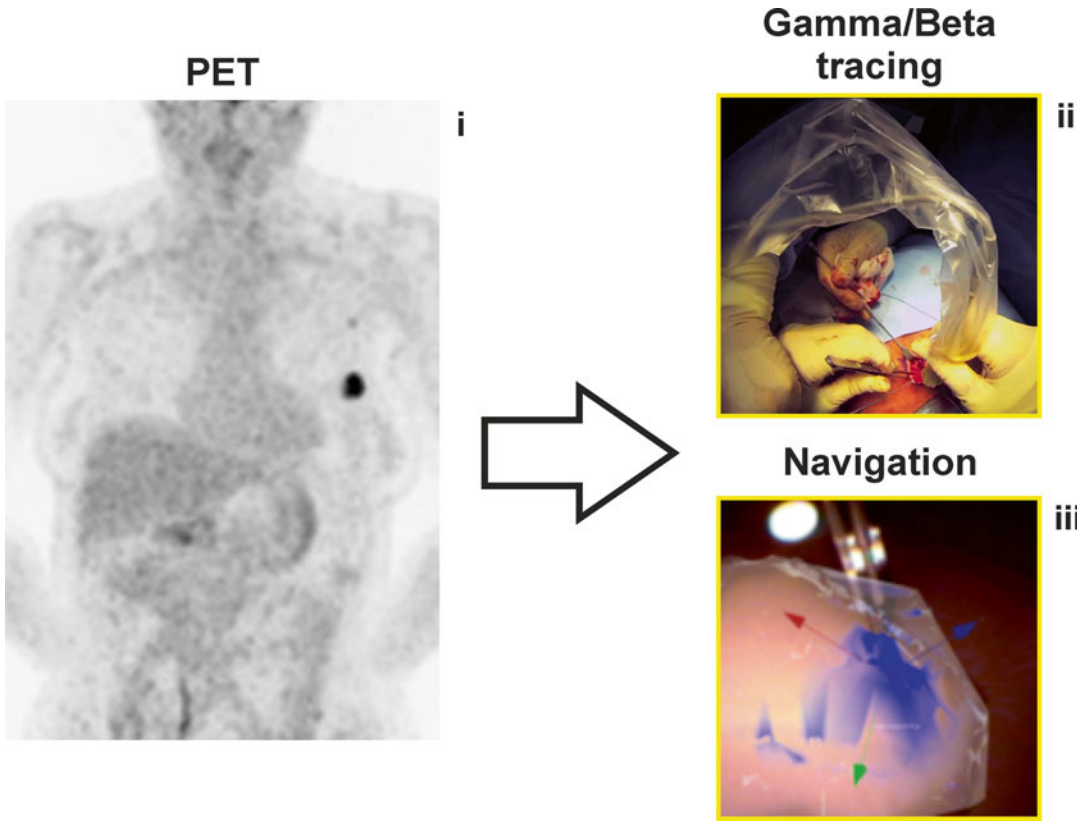

Fig. 5.9 Application of β-emitters in RGS. (*i*) Whole body nuclear imaging by PET; (*ii*) intraoperative gamma and beta tracing with acoustic probes; (*iii*) virtual navigation based on preoperative PET imaging or intraoperative freehand β-detection

medical personnel (Table 5.2). ^{18}F is generated by proton irradiation of $H_2{}^{18}O$ or $^{18}O_2$ [121] and can be covalently incorporated in radiotracers via nucleophilic or electrophilic introductions, for which multiple reagents have been developed, e.g., [^{18}F]-F$^-$-kryptofix [121]. An alternative approach would be to incorporate ^{18}F (in the form of aluminum fluoride) in a chelate (NOTA), thereby allowing labeling of tracers by simple mixing just before administration [122].

2-Deoxy-2-(^{18}F)fluoro-D-glucose (^{18}F-FDG) (Fig. 5.3), a glucose in which the hydroxyl group at the 2-position is replaced via nucleophilic substitution by ^{18}F, is the most widely applied tracer in modern nuclear medicine and can be used to highlight areas with a high metabolic activity. ^{18}F-FDG has also been applied for RGS approaches because of its widespread use and tumor accumulating characteristics. Yet, due to its short half-life, the interval between tracer administration and surgery is limited. Furthermore certain (metabolic active) organs and tissues are known to accumulate ^{18}F-FDG, e.g., the heart, brains, and bladder, which may obscure detection of lesions in these anatomies.

Early ^{18}F-FDG RGS studies have been performed with non-optimized gamma cameras (detection windows around 124, 150, 200, and 255 KeV), resulting in low-radiation detection [14]. More optimized high-energy gamma detectors have later been used to locate, e.g., colorectal tumors and lymphoma, which resulted in the removal of non-palpable and difficult to locate lesions [120, 123–125]. Next to high-energy gamma detectors, also β-sensitive probes were applied [120]. Although the authors claim the selective detection of β-particles, the detection up to 6 cm raises some questions about the selectivity of the probe [120].

A case study has also been reported regarding RGS with ^{18}F-L-DOPA (Fig. 5.3). Increased uptake of ^{18}F-L-DOPA in tumors is caused by the upregulation of amino-acid transporters, to supply the malignancy in their demand for nutrients. The application of ^{18}F-L-DOPA in RGS with a high-energy gamma detector resulted in the successful removal of multiple neuroendocrine tumors and metastases [13].

5.3.2.2 68-Gallium

^{68}Ga is a positron emitter that emits β$^+$-particles of 1.9 MeV and has a half-life of 67.7 min. We were not able to find information about the effective dose for patients; a high radiation burden can be expected based on the high-energy β$^+$-particles and the 511 keV photons generated by positron annihilation. For the medical personnel the radiation burden is caused by the 511 keV photons and is therefore similar for most β$^+$-emitters (Table 5.2). ^{68}Ga can be eluted from a ^{68}Ga-generator; a stationary phase with absorbed ^{68}Ge is eluted with an acidic mobile phase, which takes the generated ^{68}Ga with it. Such a generator can be maintained at location, e.g., a nuclear facility in a medical center. For RGS applications similar advantages and disadvantages can be expected as described above for ^{18}F. From the chemical perspective, ^{68}Ga can, however, be more easily incorporated in a radiotracer via chelation by a bifunctional chelate conjugated to the targeting moiety. DOTA has been the chelate of choice in the clinically used ^{68}Ga-based radiotracers, although other and possibly better chelates are available, e.g., NOTA and TRAP [126, 127]. Due to the requirement of a chelate in combination with a short half-live, ^{68}Ga has been predominantly used in combination with peptide constructs. For RGS applications, ^{68}Ga was incorporated in the somatostatin analogues DOTA-NOC and DOTA-octreotate (DOTA-TATE) (Fig. 5.4). These radiotracers have been successfully used for RGS towards gastroenteropancreatic neuroendocrine tumors. In 9 patients, the RGS approach with a high-energy gamma detector allowed detection of 94 % of lesions (up to 5 mm tumors) compared to 69 % by preoperative PET imaging and 50 % by surgical palpation [27].

5.3.2.3 89-Zirconium

^{89}Zr has both β$^+$- and γ-emissions of 389 and 909 keV, respectively, and has a half-life of 78.4 h. Due to the high-energy emissions and medium half-life, ^{89}Zr causes a considerable radiation burden for the patient. Also the radiation dose for the medical personnel is slightly higher compared to other β$^+$-emitters due to the additional γ-emission. ^{89}Zr is produced by proton irradiation of ^{89}Y and can be incorporated in a

radiotracer via the bifunctional chelate desferrioxamine.

In a pilot study with ^{89}Zr-desferioxamine-nanocolloid (Fig. 5.2) for SLN mapping by Heuveling et al., a higher resolution in the preoperative nuclear imaging (PET vs SPECT) was observed [28]. The authors claim that, by using a β-selective probe, RGS based on ^{89}Zr-desferrioxamine-nanocolloid should provide a similar or better intraoperative detection, compared to ^{99m}Tc-nanocolloid, especially for localization of a SLN near the injection site. This was however not (yet) shown.

5.3.2.4 124-Iodine

^{124}I is a γ- and β^+-emitter that emits photons of 0.6 and 1.7 MeV and β^+-particles of 1.5 and 2.1 MeV. ^{124}I has a half-life of 4.18 days. Due to its little use in (clinical) research, we were not able to find information about the effective dose for patients. A high radiation burden can be expected based on the high-energy emissions and long half-life. The exposure for medical personnel is considerable (Table 5.2). ^{124}I is produced by proton irradiation of ^{124}Te. The conjugation chemistry for this isotope is similar to that of the other iodine isotopes reported above.

Although ^{124}I is mainly used for PET imaging, this isotope has been applied in RIGS tracing both the positrons and the high-energy photons (511 keV) originating from ^{124}I-labeled antibodies against A33 transmembrane glycoprotein (huA33) and against carbonic anhydrase IX (cG250) [33]. Detection was performed by both a high-energy gamma detector and a β-selective detector. In four patients a high correlation between γ- and β^+-detection was determined and the authors claim that the β-probe showed a higher tumor to background signal compared to the high-energy gamma probe.

5.3.3 Electron Radiation

β^--particle or electron-emitting radionuclides have been applied for RGS for two reasons. The first reason is the clinical application of β^--emitters for radiotherapy, which allows RGS toward the residual lesion based on other emissions of the radionuclide. The second reason for using a (pure) β^--emitter in combination with a β^--specific detector for RGS is the very limited range of β^--particles in tissue. Any uptake in nearby healthy tissue or radiation of a nearby injection site is attenuated before reaching the detector. This would result in a lower background and a better delineation of the margins around the lesion of interest. Unfortunately a (pure) β^--emitter does not allow preoperative whole body imaging for surgical planning and an approximate location of the lesion of interest has to be known to be able to locate it with a β^--specific probe.

5.3.3.1 32-Phosphorus

^{32}P emits β^--particles of 690 keV and has a half-life of 14.3 days. Due to its limited use in clinical research, we were not able to find information about the effective dose for patients or medical personnel. ^{32}P is produced by neutron irradiation of ^{32}S. One of the first studies on RGS reported on in 1949, applying a Geiger-Müller device, was performed with ^{32}P-PO_4^{2-} (Fig. 5.3). The accumulation and turnover of the phosphate ion were found higher in tumor tissue compared to healthy brain tissue, thereby allowing the identification of cerebral gliomas in 14 patients [24]. Due to its β^--emission, ^{32}P has not been widely applied for RGS, but for research purposes, multiple methods are available to label all kind of tracers with this isotope [128, 129].

5.3.3.2 90-Yttrium

^{90}Y emits β^--particles of 2.3 MeV and has a half-life of 64 h. The high-energy β^-emission results in a high radiation burden for the patient, and therefore, this isotope is mainly used for therapeutic purposes. However, the additional X-ray generation and the use of high therapeutic dosages cause considerable radiation exposure for the medical personnel. ^{90}Y is a decay product of ^{90}Sr, which is produced upon uranium and plutonium fission in nuclear power plants. Small-scale ^{90}Y generators based on ^{90}Sr have been developed, which can be used for the production of ^{90}Y with high specific activity [130]. These

generators can be operated at the local nuclear facility of medical centers. Although ^{90}Y is almost purely a β^--emitter, SPECT imaging has been performed based on Bremsstrahlung, which originates from the loss of kinetic energy from the high-energy electrons (β^-) resulting in the emission of photons [131]. Also PET imaging is possible due to the rare (1 in 32 million transitions) β^-/β^+-pair formation, of which the β^+ can subsequently annihilate with an electron to produce two photons of 511 keV [132, 133]. ^{90}Y can be incorporated in radiotracers by binding it to the bifunctional chelate DOTA, which can be conjugated to a variety of targeting moieties.

Recently the use of a β^--specific probe in combination with the ^{90}Y-labeled somatostatin analogue DOTA-TOC (Fig. 5.4) was suggested for the detection of meningioma and high-grade glioma [29]. In this study, PET imaging was performed with ^{68}Ga-DOTA-TOC and provided quantitative information about the uptake of the tracer. Based on this information, the required dosage of ^{90}Y-DOTA-TOC was calculated to discriminate the lesion of interest from the surrounding healthy tissue with a β^--specific probe [29]. Based on this preoperative ^{68}Ga-based imaging and calculations, the authors concluded that RGS based on ^{90}Y-DOTA-TOC should be possible [29].

5.4 Hybrid Imaging and Detection Platforms (Table 5.3)

Hybrid imaging combines two imaging modalities, e.g., nuclear and luminescence imaging, in a single approach. It was already introduced in 1948 by Moore et al. who radiolabeled diiodofluorescein, resulting in a tracer that has both a nuclear and a fluorescent component. Luminescence imaging in the clinic has been performed based on fluorescence and Cherenkov luminescence (CL) and can provide high-resolution imaging in the operating theatre to aid the surgeon in detecting the lesion of interest (Fig. 5.11b). The advantage of luminescence-guided surgery over radioguided surgery lies in the limited tissue attenuation of visible light [138]; like with β^--particle or electron-emitting radionuclides, imaging of optical signals is less hindered by background signals originating from the injection site or from tracer accumulation in the vicinity of the lesion of interest. However, due to the limited tissue penetration of light (<1 cm) [138], luminescence imaging is not suitable for whole body imaging. Therefore, the application of a radio- and luminescent tracer combines the best of both worlds.

Two subclasses of hybrid tracers have been reported for clinical use, being the combination of a radionuclide and a fluorescent label on a single tracer (Fig. 5.11a) or the detection of the Cherenkov luminescence (CL) emitted by β^+/β^--emitting isotopes (Fig. 5.11b). Fluorescence imaging is based on the excitation of a fluorescent label with light, which results in the emission of light of a longer wavelength. The advantage of fluorescence imaging is that it provides real-time high-resolution information. Yet, fluorescence imaging requires the addition of a fluorescent label to the imaging tracer, the excitation light has to be blocked from reaching the camera, and background fluorescence can occur originating from endogenous fluorophores.

Cherenkov photons (Cherenkov Luminescence; CL) originate from charged particles (β+ /β–) that travel through a medium faster than the speed of light in that same medium. CL occurs in tissue when the emitted charged particles have energies higher than 0.21 MeV. The intensity of CL is around three orders of

Table 5.3 Optical characteristics of clinically applied hybrid tracers

Optical component	λ_{exc} (nm)	λ_{em} (nm)	Example of use during RGS
Diiodofluorescein	488	515	Moore et al. [134]
I-Methylene blue	670	680	Cundiff et al. [135]
ICG-nanocolloid	780	820	van der Poel et al. [136]
Cherenkov luminescence	na	>200	Spinelli et al. [137]

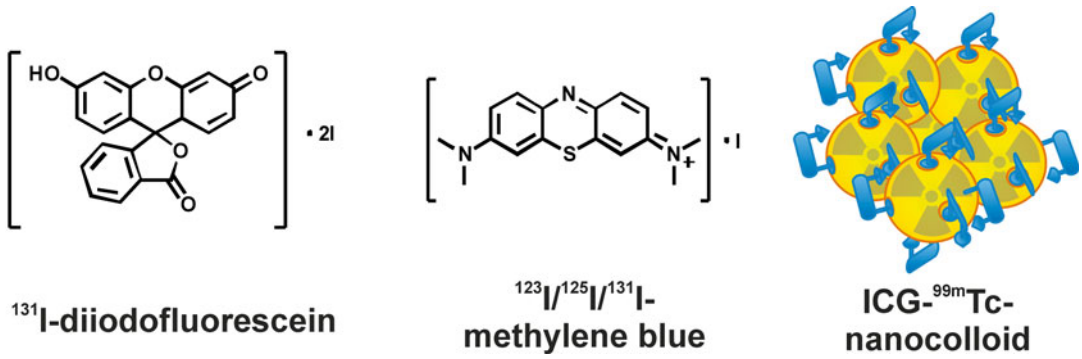

Fig. 5.10 Hybrid imaging tracers applied in RGS

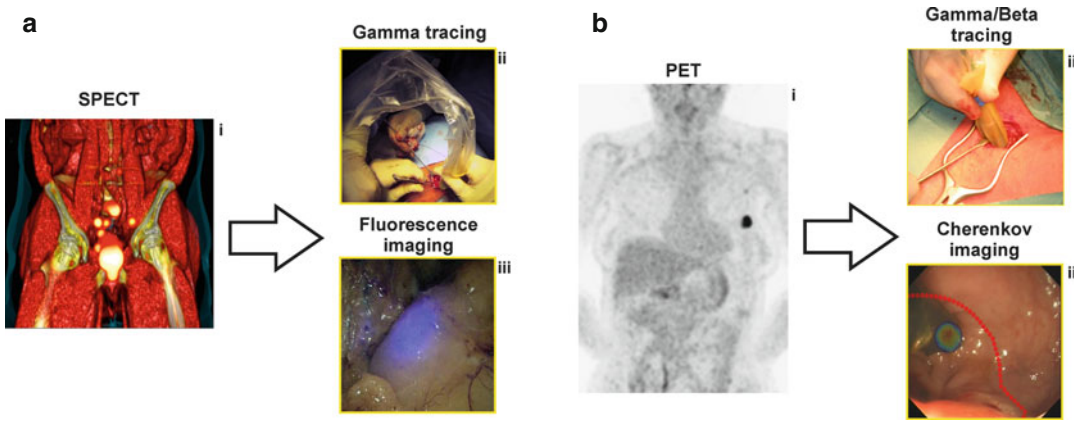

Fig. 5.11 Application of hybrid tracers in RGS. (**a**) Hybrid tracers combining nuclear imaging with fluorescence imaging: (*i*) whole body nuclear imaging; (*ii*) intraoperative tracing with acoustic probe; (*iii*) intraoperative fluorescence imaging. Real-time fluorescence overlaid with white-light image. (**b**) Hybrid imaging based on Cherenkov luminescence emitted by β^+/β^--emitting isotopes: (*i*) whole body nuclear imaging; (*ii*) intraoperative tracing with acoustic probe; (*iii*) intraoperative optical imaging. CL images overlaid with white-light photograph. *With kind permission from Springer Science and Business Media* [139]

magnitude lower than that obtained with fluorescence imaging, but during the decay of the isotope, it provides a continuous spectrum with peak emission in the UV range [140]. The advantage of CL is that no additional label is required next to the β -particle emitting radionuclide and that there is virtually no background signal because no external excitation light is required. However, since the CL intensity is tracer dose dependent, it may negatively influence the dose received by the patient and surgical staff [23]. Furthermore, low signal intensity means long acquisition times and absolute darkness are needed to generate an image and thus real-time guidance is not possible.

The earliest example of a hybrid tracer of the first subclass is ^{131}I-diiodofluorescein (Fig. 5.10), which was reported by Moore et al. in 1948. Fluorescein was already reported for the detection of malignant tissue by UV-light irradiation and visible detection of the fluorescence ($\lambda_{em} = 520$ nm) by eye [112]. By radioiodination, this fluorescent tracer could be detected using a Geiger-Müller tube [110, 111]. Both the radiosignal and the fluorescence detection could be used to localize brain lesions [134].

The radioiodinated (^{123}I, ^{125}I, and ^{131}I) derivative of methylene blue (Fig. 5.10), a blue dye commonly used for optical visualization of the lymphatic ducts, has been used for lymphatic

mapping and RGS toward SLN(s), which resulted in the successful removal [135, 141–143]. Although methylene blue was shown to possess fluorescence properties [144], these were not exploited within the clinical studies.

For SLN biopsy procedures, the hybrid radioactive and fluorescent tracer indocyanine green (ICG)-^{99m}Tc-nanocolloid was introduced (Fig. 5.10). The tracer was formed via the noncovalent interaction between the near-infrared fluorescent dye ICG and the albumin components of ^{99m}Tc-nanocolloid [6, 136]. An early reproducibility study showed the behavior of the hybrid tracer being identical to its parental compound ^{99m}Tc-nanocolloid [145]. Next to preoperative SLN mapping, intraoperative radioguidance and fluorescence guidance to the SLN(s) were facilitated. The latter allowing the optical verification of the location of the SLN, which was not possible with the parental compound [146, 147]. The addition of real-time fluorescence imaging during the RGS procedure was considered especially valuable during the detection of SLNs close to the injection site of the radiocolloid [148], and enabled optical detection of SLN(s) failed to accumulated the traditionally used blue dye [146].

Cherenkov photons originate from charged particles (β^+/β^-) that travel through a medium faster than the speed of light in that same medium. CL occurs in tissue when the emitted charged particles have energies higher than 0.21 MeV. The intensity of CL is around three orders of magnitude lower than that obtained with fluorescence imaging, but during the decay of the isotope, it provides a continuous spectrum with peak emission in the UV range [140]. The advantage of CL is that no additional label is required next to the β-particle emitting radionuclide and that there is virtually no background signal because no external excitation light is required. However, since the CL intensity is tracer dose dependent, it may negatively influence the dose received by the patient and surgical staff [23]. Furthermore, low signal intensity means long acquisition times and absolute darkness are needed to generate an image and thus real-time guidance is not possible.

For CL imaging, all β^+- and β^--emitters used in clinical practice can potentially be used. This said, the amount of clinical reports on CL imaging is limited. Recently clinical studies with ^{131}I (for thyroid) and ^{18}F-FDG (for various malignancies) have been reported, showing the clinical feasibility of CL imaging [137, 139, 149]. In these studies superficial lesions were visualized through the skin. Technical camera development for CL imaging is moving toward endoscopic use and a laparoscopic camera for CL imaging was recently evaluated in four patients with colorectal cancer [139].

5.5 Future Perspectives

Although this chapter discusses radiotracers that have already been applied for RGS in patients, in principle all clinically used radiotracers can be applied for RGS. This includes also the tracers that are currently investigated for diagnostic imaging purposes, such as ^{18}F-fluorothymidine (^{18}F-FLT; visualizes cell proliferation), ^{18}F- and ^{99m}Tc-annexin V (visualizes cell apoptosis/necrosis), ^{68}Ga-prostate-specific membrane antigen ligand (^{68}Ga-PSMA; visualizes the prostate-specific membrane antigen), ^{99m}Tc-etarfolatide (visualizes epithelial tumor cells), and various antibodies labeled with ^{89}Zr [150–152]. Also in the preclinical field, several promising radio- and hybrid tracers are being developed that might be applicable in RGS and image-guided surgery [153–158]. Although the recent reemergence of image-guided surgery has boosted the preclinical activities regarding tracer development for this application, the "from molecule to man" translation of these activities remains limited.

Interesting recent developments in the choice of radionuclides for RGS are the steps toward the application of β^+- (e.g., ^{18}F and ^{89}Zr) and β^--emitters (^{90}Y) for RGS. Especially the selective detection of the β-particles can potentially improve the resolution in RGS. However, the application of these radionuclides increases the radiation dosages obtained by patients (both β^-- and β^+-emitters) and medical personnel (mainly β^+-emitters). This aspect needs to be resolved in order to implement such RGS procedures in an everyday clinical practice. One suggestion would

be to improve the specificity and especially the sensitivity of the imaging modalities, both nuclear and optical, which would allow the application of lower dosages of these radiotracers.

5.6 Concluding Remarks

As can be concluded from the described applications of radioisotopes in RGS, the most used radioisotopes are ^{99m}Tc (radiocolloids and ^{99m}Tc-sestamibi), ^{111}In (^{111}In-somatostatin analogues), and ^{125}I (^{125}I-MIBG and ^{125}I-labeled antibodies). This originates mainly from their easy availability, their preferred medium to low-energy photon emission, and their ease of incorporation into radiotracers. Interesting new developments are focusing on surgical guidance toward β-emitters and the inclusion of optical guidance methods. A critical point in the development of new RGS procedures and the use of certain radionuclides is the radiation exposure of the surgical staff. Especially the need for isotopes with high-energy emissions may limit the clinical application due to restrictions in the radiation exposure of the medical personnel.

Acknowledgments This work was financially supported by a Netherlands Organisation for Scientific Research VIDI grant (NWO; STW BGT 11272).

References

1. Brouwer OR, Buckle T, Bunschoten A, Kuil J, Vahrmeijer AL, Wendler T, Valdes-Olmos RA, van der Poel HG, van Leeuwen FWB. Image navigation as a means to expand the boundaries of fluorescence-guided surgery. Phys Med Biol. 2012;57(10): 3123–36.
2. Uren RF. Lymphatic drainage of the skin. Ann Surg Oncol. 2004;11(3 Suppl):179S–85.
3. Ege GN. Internal mammary lymphoscintigraphy. The rationale, technique, interpretation and clinical application: a review based on 848 cases. Radiology. 1976;118(1):101–7.
4. Henze E, Schelbert HR, Collins JD, Najafi A, Barrio JR, Bennett LR. Lymphoscintigraphy with Tc-99m-labeled dextran. J Nucl Med. 1982;23(10):923–9.
5. Sarin H. Physiologic upper limits of pore size of different blood capillary types and another perspective on the dual pore theory of microvascular permeability. J Angiogenes Res. 2010;2:14.
6. van Leeuwen AC, Buckle T, Bendle G, Vermeeren L, Valdes Olmos R, van der Poel HG, van Leeuwen FWB. Tracer-cocktail injections for combined pre- and intraoperative multimodal imaging of lymph nodes in a spontaneous mouse prostate tumor model. J Biomed Opt. 2011;16(1):016004.
7. Mariani G, Erba P, Villa G, Gipponi M, Manca G, Boni G, Buffoni F, Castagnola F, Paganelli G, Strauss HW. Lymphoscintigraphic and intraoperative detection of the sentinel lymph node in breast cancer patients: the nuclear medicine perspective. J Surg Oncol. 2004;85(3):112–22.
8. Van den Berg NS, Buckle T, Kleinjan GI, Klop WM, Horenblas S, Van Der Poel HG, Valdes-Olmos RA, Van Leeuwen FI. Hybrid tracers for sentinel node biopsy. Q J Nucl Med Mol Imaging. 2014;58(2):193–206.
9. Pouw B, de Wit-van der Veen LJ, Stokkel MP, Loo CE, Vrancken Peeters MJ, Valdes Olmos RA. Heading toward radioactive seed localization in non-palpable breast cancer surgery? A meta-analysis. J Surg Oncol. 2015;111(2):185–91.
10. Thind CR, Tan S, Desmond S, Harris O, Ramesh HS, Chagla L, Ray A, Audisio R, SNOLL. Sentinel node and occult (impalpable) lesion localization in breast cancer. Clin Radiol. 2011;66(9):833–9.
11. Lavoue V, Nos C, Clough KB, Baghaie F, Zerbib E, Poulet B, Lefrere Belda MA, Ducellier A, Lecuru F. Simplified technique of radioguided occult lesion localization (ROLL) plus sentinel lymph node biopsy (SNOLL) in breast carcinoma. Ann Surg Oncol. 2008;15(9):2556–61.
12. Heij HA, Rutgers EJ, de Kraker J, Vos A. Intraoperative search for neuroblastoma by MIBG and radioguided surgery with the gamma detector. Med Pediatr Oncol. 1997;28(3):171–4.
13. Arbizu J, Rodriguez-Fraile M, Dominguez-Prado I, Garrastachu P, Rotellar F, Sangro B, Richter JA. Whole body 18fluoro-L-dopa PET-CT: a useful tool for location and surgical guidance in primary carcinoid tumours. Eur J Nucl Med Mol Imaging. 2008;35(8):1577.
14. Desai DC, Arnold M, Saha S, Hinkle G, Soble D, Fry J, DePalatis LR, Mantil J, Satter M, Martin Jr EW. Correlative whole-body FDG-PET and intraoperative gamma detection of FDG distribution in colorectal cancer. Clin Positron Imaging. 2000;3(5): 189–96.
15. Krag DN, Ford PV, Patel M, Schneider PD, Goodnight Jr JE. A simplified technique to resect abnormal bony radiolocalizations using a gamma counter. Surg Oncol. 1992;1(5):371–7.
16. Martin DT, Hinkle GH, Tuttle S, Olsen J, Nabi H, Houchens D, Thurston M, Martin Jr EW. Intraoperative radioimmunodetection of colorectal tumors with a hand-held radiation detector. Am J Surg. 1985;150: 672–5.
17. Agnese DM, Abdessalam SF, Burak Jr WE, Arnold MW, Soble D, Hinkle GH, Young D, Khazaeli

MB, Martin Jr EW. Pilot study using a humanized CC49 monoclonal antibody (HuCC49DeltaCH2) to localize recurrent colorectal carcinoma. Ann Surg Oncol. 2004;11(2):197–202.
18. Nieroda CA, Milenic DE, Colcher D, Schlom J. Monoclonal antibodies for use in radioimmunoguided surgery (RIGS). In: Martin Jr EW, editor. Radioimmunoguided surgery (RIGS) in the detection of colorectal cancer. Austin: R. G. Landes Company; 1994. p. 7–27.
19. de Labriolle-Vaylet C, Cattan P, Sarfati E, Wioland M, Billotey C, Brocheriou C, Rouvier E, de Roquancourt A, Rostene W, Askienazy S, Barbet J, Milhaud G, Gruaz-Guyon A. Successful surgical removal of occult metastases of medullary thyroid carcinoma recurrences with the help of immunoscintigraphy and radioimmunoguided surgery. Clin Cancer Res. 2000;6(2):363–71.
20. Sharkey RM, Chang CH, Rossi EA, McBride WJ, Goldenberg DM. Pretargeting: taking an alternate route for localizing radionuclides. Tumour Biol. 2012;33(3):591–600.
21. Nelson AL. Antibody fragments: hope and hype. MAbs. 2010;2(1):77–83.
22. van Leeuwen FWB, Hardwick JC, van Erkel AR. Luminescence-based imaging approaches in the field of interventional (molecular) imaging. Radiology. 2015;276(1):12–29.
23. Chin PTK, Welling MM, Meskers SC, Valdes Olmos RA, Tanke H, van Leeuwen FWB. Optical imaging as an expansion of nuclear medicine: Cerenkov-based luminescence vs fluorescence-based luminescence. Eur J Nucl Med Mol Imaging. 2013;40(8):1283–91.
24. Selverstone B, Sweet WH, Robinson CV. The clinical use of radioactive phosphorus in the surgery of brain tumors. Ann Surg. 1949;130(4):643–51.
25. Woolfenden JM, Nevin WS, Barber HB, Donahue DJ. Lung cancer detection using a miniature sodium iodide detector and cobalt-57 bleomycin. Chest. 1984;85(1):84–8.
26. Schattner A, Cohen A, Wolfson L, Melloul M. Unexplained systemic symptoms and Gallium-67 – guided decisions. Am J Med Sci. 2001;321(3):198–200.
27. Kaemmerer D, Prasad V, Daffner W, Haugvik SP, Senftleben S, Baum RP, Hommann M. Radioguided surgery in neuroendocrine tumors using Ga-68-labeled somatostatin analogs: a pilot study. Clin Nucl Med. 2012;37(2):142–7.
28. Heuveling DA, van Schie A, Vugts DJ, Hendrikse NH, Yaqub M, Hoekstra OS, Karagozoglu KH, Leemans CR, van Dongen GA, de Bree R. Pilot study on the feasibility of PET/CT lymphoscintigraphy with 89Zr-nanocolloidal albumin for sentinel node identification in oral cancer patients. J Nucl Med. 2013;54(4):585–9.
29. Collamati F, Pepe A, Bellini F, Bocci V, Chiodi G, Cremonesi M, De Lucia E, Ferrari ME, Frallicciardi PM, Grana CM, Marafini M, Mattei I, Morganti S, Patera V, Piersanti L, Recchia L, Russomando A, Sarti A, Sciubba A, Senzacqua M, Camillocci ES, Voena C, Pinci D, Faccini R. Toward radioguided surgery with beta(−) decays: uptake of a somatostatin analogue, DOTATOC, in meningioma and high-grade glioma. J Nucl Med. 2015;56(1):3–8.
30. Gommans GM, Gommans E, van der Zant FM, Teule GJ, van der Schors TG, de Waard JW. 99mTc Nanocoll: a radiopharmaceutical for sentinel node localisation in breast cancer – in vitro and in vivo results. Appl Radiat Isot. 2009;67(9):1550–8.
31. Panareo S, Carcoforo P, Lanzara S, Corcione S, Bagatin E, Casali M, Costanzo A, Basaglia E, Feggi LM. Radiolabelled somatostatin analogs for diagnosis and radio-guided surgery of neuroendocrine breast cancer undetectable with conventional imaging procedures. Breast. 2008;17(1):111–4.
32. Gallowitsch HJ, Fellinger J, Mikosch P, Kresnik E, Lind P. Gamma probe-guided resection of a lymph node metastasis with I-123 in papillary thyroid carcinoma. Clin Nucl Med. 1997;22(9):591–2.
33. Strong VE, Humm J, Russo P, Jungbluth A, Wong WD, Daghighian F, Old L, Fong Y, Larson SM. A novel method to localize antibody-targeted cancer deposits intraoperatively using handheld PET beta and gamma probes. Surg Endosc. 2008;22(2):386–91.
34. Hinkle GH, Laven DL. Radionuclides. In: Martin Jr EW, editor. Radioimmunoguided Surgery (RIGS) in the detection and treatment of colorectal cancer. Austin: R. G. Landes Company; 1994. p. 29–39.
35. Jager W, Feistel H, Paterok EM, Ronay G, Tulusan AH, Wolf F, Lang N. Resection guided by antibodies (REGAJ): a diagnostic procedure during second-look operation in ovarian cancer patients. Br J Cancer Suppl. 1990;10:18–20.
36. Ubhi CS, Hardy JG, Pegg CA. Mediastinal parathyroid adenoma: a new method of localization. Br J Surg. 1984;71(11):859–60.
37. Bartholoma MD, Louie AS, Valliant JF, Zubieta J. Technetium and gallium derived radiopharmaceuticals: comparing and contrasting the chemistry of two important radiometals for the molecular imaging era. Chem Rev. 2010;110(5):2903–20.
38. Dewanjee MK. The chemistry of 99mTc-labeled radiopharmaceuticals. Semin Nucl Med. 1990;20(1):5–27.
39. Hetrakul N, Civelek AC, Stagg CA, Udelsman R. In vitro accumulation of technetium-99m-sestamibi in human parathyroid mitochondria. Surgery. 2001;130(6):1011–8.
40. Nazari B, Azizmohammadi Z, Rajaei M, Karami M, Javadi H, Assadi M, Asli IN. Role of 99mTc-ubiquicidin 29–41 scintigraphy to monitor antibiotic therapy in patients with orthopedic infection: a preliminary study. Nucl Med Commun. 2011;32(8):745–51.
41. Eshima D, Eshima LA, Gotti NM, Herda SC, Algozine CA, Burris TG, Vansant JP, Alazraki NP, Taylor AT. Technetium-99m-sulfur colloid for lymphoscintigraphy: effects of preparation parameters. J Nucl Med. 1996;37(9):1575–8.

42. Vera DR, Wallace AM, Hoh CK, Mattrey RF. A synthetic macromolecule for sentinel node detection: (99m)Tc-DTPA-mannosyl-dextran. J Nucl Med. 2001;42(6):951–9.
43. Hubalewska-Dydejczyk A, Kulig J, Szybinski P, Mikolajczak R, Pach D, Sowa-Staszczak A, Fross-Baron K, Huszno B. Radio-guided surgery with the use of [99mTc-EDDA/HYNIC]octreotate in intra-operative detection of neuroendocrine tumours of the gastrointestinal tract. Eur J Nucl Med Mol Imaging. 2007;34(10):1545–55.
44. Linehan DC, Hill AD, Tran KN, Yeung H, Yeh SD, Borgen PI, Cody 3rd HS. Sentinel lymph node biopsy in breast cancer: unfiltered radioisotope is superior to filtered. J Am Coll Surg. 1999;188(4):377–81.
45. Higashi H, Natsugoe S, Uenosono Y, Ehi K, Arigami T, Nakabeppu Y, Nakajo M, Aikou T. Particle size of tin and phytate colloid in sentinel node identification. J Surg Res. 2004;121(1):1–4.
46. Tsopelas C. Particle size analysis of (99m)Tc-labeled and unlabeled antimony trisulfide and rhenium sulfide colloids intended for lymphoscintigraphic application. J Nucl Med. 2001;42(3):460–6.
47. Hodgson N, Zabel P, Mattar AG, Engel CJ, Girvan D, Holliday R. A new radiocolloid for sentinel node detection in breast cancer. Ann Surg Oncol. 2001; 8(2):133–7.
48. Lombardi A, Nigri G, Scopinaro F, Maggi S, Mattei M, Bonifacino A, Parisella M, Soluri A, Amanti C. High-resolution, handheld camera use for occult breast lesion localization plus sentinel node biopsy (SNOLL): A single-institution experience with 186 patients. Surgeon. 2015;13(2):69–72.
49. Mirzaei S, Rodrigues M, Hoffmann B, Knoll P, Riegler-Keil M, Kreuzer W, Salzer H, Kohn H, Polyak A, Janoki GA. Sentinel lymph node detection with large human serum albumin colloid particles in breast cancer. Eur J Nucl Med Mol Imaging. 2003;30(6):874–8.
50. Jeschke S, Beri A, Grull M, Ziegerhofer J, Prammer P, Leeb K, Sega W, Janetschek G. Laparoscopic radioisotope-guided sentinel lymph node dissection in staging of prostate cancer. Eur Urol. 2008;53(1):126–32.
51. Reasbeck PG, Manktelow A, McArthur AM, Packer SG, Berkeley BB. An evaluation of pelvic lymphoscintigraphy in the staging of colorectal carcinoma. Br J Surg. 1984;71(12):936–40.
52. Xavier NL, Amaral BB, Cerski CT, Fuchs SC, Spiro BL, Oliveira OL, Menke CH, Biazus JV, Cavalheiro JA, Schwartsmann G. Sentinel lymph node identification and sampling in women with early breast cancer using 99m Tc labelled dextran 500 and patent blue V dye. Nucl Med Commun. 2001;22(10):1109–17.
53. Marcinow AM, Hall N, Byrum E, Teknos TN, Old MO, Agrawal A. Use of a novel receptor-targeted (CD206) radiotracer, 99mTc-tilmanocept, and SPECT/CT for sentinel lymph node detection in oral cavity squamous cell carcinoma: initial institutional report in an ongoing phase 3 study. JAMA Otolaryngol Head Neck Surg. 2013;139(9):895–902.
54. Sondak VK, King DW, Zager JS, Schneebaum S, Kim J, Leong SP, Faries MB, Averbook BJ, Martinez SR, Puleo CA, Messina JL, Christman L, Wallace AM. Combined analysis of phase III trials evaluating [(9)(9)mTc]tilmanocept and vital blue dye for identification of sentinel lymph nodes in clinically node-negative cutaneous melanoma. Ann Surg Oncol. 2013;20(2):680–8.
55. Wallace AM, Han LK, Povoski SP, Deck K, Schneebaum S, Hall NC, Hoh CK, Limmer KK, Krontiras H, Frazier TG, Cox C, Avisar E, Faries M, King DW, Christman L, Vera DR. Comparative evaluation of [(99m)tc]tilmanocept for sentinel lymph node mapping in breast cancer patients: results of two phase 3 trials. Ann Surg Oncol. 2013;20(8):2590–9.
56. Aras G, Gultekin SS, Kucuk NO, Demirer S, Tug T. Intraoperative gamma probe guidance with 99mTc-pertechnetate in the completion thyroidectomy. Ann Nucl Med. 2009;23(5):421–6.
57. Mandalapu BP, Amato M, Stratmann HG. Technetium Tc 99m sestamibi myocardial perfusion imaging: current role for evaluation of prognosis. Chest. 1999; 115(6):1684–94.
58. Duarte GM, Cabello C, Torresan RZ, Alvarenga M, Telles GH, Bianchessi ST, Caserta N, Segala SR, de Lima MC, Etchebehere EC, Camargo EE. Radioguided Intraoperative Margins Evaluation (RIME): preliminary results of a new technique to aid breast cancer resection. Eur J Surg Oncol. 2007;33(10):1150–7.
59. Vilela Filho O, Carneiro Filho O. Gamma probe-assisted brain tumor microsurgical resection: a new technique. Arq Neuropsiquiatr. 2002;60:1042–7.
60. Martinez DA, King DR, Romshe C, Lozano RA, Morris JD, O'Dorisio MS, Martin Jr EW. Intraoperative identification of parathyroid gland pathology: a new approach. J Pediatr Surg. 1995;30(9):1306–9.
61. Placzkowski K, Christian R, Chen H. Radioguided parathyroidectomy for recurrent parathyroid cancer. Clin Nucl Med. 2007;32(5):358–60.
62. Ikeda Y, Takayama J, Takami H. Minimally invasive radioguided parathyroidectomy for hyperparathyroidism. Ann Nucl Med. 2010;24(4):233–40.
63. Garcia-Talavera P, Gonzalez-Selma ML, Ruiz M, Gamazo C, Sainz-Esteban A, Villanueva JG, Olmos R. The value of early SPECT/CT and handheld gamma-camera in radio-guided surgery: a case of a hard-to-locate parathyroid adenoma. Clin Nucl Med. 2014;39(11):1009–11.
64. Mariani G, Gulec SA, Rubello D, Boni G, Puccini M, Pelizzo MR, Manca G, Casara D, Sotti G, Erba P, Volterrani D, Giuliano AE. Preoperative localization and radioguided parathyroid surgery. J Nucl Med. 2003;44(9):1443–58.
65. Al-Saeedi F. Role of 99mTc-(V)DMSA in detecting tumor cell proliferation. Anal Chem Insights. 2007; 2:81–3.
66. Adams S, Acker P, Lorenz M, Staib-Sebler E, Hor G. Radioisotope-guided surgery in patients with pheochromocytoma and recurrent medullary thyroid

carcinoma: a comparison of preoperative and intraoperative tumor localization with histopathologic findings. Cancer. 2001;92(2):263–70.
67. Povoski SP, Neff RL, Mojzisik CM, O'Malley DM, Hinkle GH, Hall NC, Murrey Jr DA, Knopp MV, Martin Jr EW. A comprehensive overview of radioguided surgery using gamma detection probe technology. World J Surg Oncol. 2009;7:11.
68. Robinson LA, Preksto D, Muro-Cacho C, Hubbell DS. Intraoperative gamma probe-directed biopsy of asymptomatic suspected bone metastases. Ann Thorac Surg. 1998;65(5):1426–32.
69. Axelsson CK, Nielsen BP, Graff J. Radioisotope-guided surgical biopsy of costal metastases in breast cancer patients. Scand J Surg. 2002;91(4):333–5.
70. von Meyenfeldt EM, Siebenga J, van der Pol HA, Schreurs WM, Hulsewe KW. Radionuclide-guided biopsy of bone lesions in cancer patients; a reliable, well-tolerated technique. Eur J Surg Oncol. 2014; 40(2):193–6.
71. Ind TE, Granowska M, Britton KE, Morris G, Lowe DG, Hudson CN, Shepherd JH. Peroperative radioimmunodetection of ovarian carcinoma using a hand-held gamma detection probe. Br J Cancer. 1994;70(6):1263–6.
72. Hladik P, Vizda J, Bedrna J, Simkovic D, Strnad L, Smejkal K, Voboril Z. Immunoscintigraphy and intraoperative radioimmunodetection in the treatment of colorectal carcinoma. Colorectal Dis. 2001;3(6):380–6.
73. Mansi L, Di Lieto E, Rambaldi PF, Bergaminelli C, Fallanca F, Vicidomini G, Cuccurullo V, Mancusi R. Preliminary experience with radioimmuno-guided surgery of primary neoplasms of the lung. Minerva Chir. 1998;53(5):369–72.
74. Mansi L, Rambaldi PF, Panza N, Esposito D, Esposito V, Pastore V. Diagnosis and radioguided surgery with 111In-pentetreotide in a patient with paraneoplastic Cushing's syndrome due to a bronchial carcinoid. Eur J Endocrinol. 1997;137(6):688–90.
75. Ohrvall U, Westlin JE, Nilsson S, Juhlin C, Rastad J, Lundqvist H, Akerstrom G. Intraoperative gamma detection reveals abdominal endocrine tumors more efficiently than somatostatin receptor scintigraphy. Cancer. 1997;80(12 Suppl):2490–4.
76. Adams S, Baum RP, Hertel A, Wenisch HJ, Staib-Sebler E, Herrmann G, Encke A, Hor G. Intraoperative gamma probe detection of neuroendocrine tumors. J Nucl Med. 1998;39(7):1155–60.
77. Grossrubatscher E, Vignati F, Dalino P, Possa M, Belloni PA, Vanzulli A, Bramerio M, Marocchi A, Rossetti O, Zurleni F, Loli P. Use of radioguided surgery with [111In]-pentetreotide in the management of an ACTH-secreting bronchial carcinoid causing ectopic Cushing's syndrome. J Endocrinol Invest. 2005;28(1):72–8.
78. Gay E, Vuillez JP, Palombi O, Brard PY, Bessou P, Passagia JG. Intraoperative and postoperative gamma detection of somatostatin receptors in bone-invasive en plaque meningiomas. Neurosurgery. 2005;57(1 Suppl):107–13; discussion 107–13.
79. Krag DN, Haseman MK, Ford P, Smith L, Taylor MH, Schneider P, Goodnight JE. Gamma probe location of 111indium-labeled B72.3: an extension of immunoscintigraphy. J Surg Oncol. 1992;51(4):226–30.
80. Muxi A, Pons F, Vidal-Sicart S, Setoain FJ, Herranz R, Novell F, Fernandez RM, Trias M, Setoain J. Radioimmunoguided surgery of colorectal carcinoma with an 111In-labelled anti-TAG72 monoclonal antibody. Nucl Med Commun. 1999;20(2):123–30.
81. Anderson RS, Eifert B, Tartt S, King P. Radioimmunoguided surgery using indium-111 capromab pendetide (PROSTASCINT) to diagnose supraclavicular metastasis from prostate cancer. Urology. 2000;56(4):669.
82. Le Doussal JM, Gruaz-Guyon A, Martin M, Gautherot E, Delaage M, Barbet J. Targeting of indium 111-labeled bivalent hapten to human melanoma mediated by bispecific monoclonal antibody conjugates: imaging of tumors hosted in nude mice. Cancer Res. 1990;50(11):3445–52.
83. Eckelman WC, Rzeszotarski WJ, Siegel BA, Kubota H, Chelliah M, Stevenson J, Reba RC. Chemical and biological properties of isolated radiolabeled bleomycin preparations. J Nucl Med. 1975;16(11):1033–7.
84. Lavender JP, Lowe J, Barker JR, Burn JI, Chaudhri MA. Gallium 67 citrate scanning in neoplastic and inflammatory lesions. Br J Radiol. 1971;44:361–6.
85. Weiner R. The role of transferrin and other receptors in the mechanism of 67Ga localization. Int J Rad Appl Instrum, Part B, Nucl Med Biol. 1990;17(1):141–9.
86. Wilbur DS. Radiohalogenation of proteins: an overview of radionuclides, labeling methods, and reagents for conjugate labeling. Bioconjum Chem. 1992;3(6):433–70.
87. Sugiura G, Kuhn H, Sauter M, Haberkorn U, Mier W. Radiolabeling strategies for tumor-targeting proteinaceous drugs. Molecules. 2014;19(2):2135–65.
88. Bourdoiseau M. Iodine radiochemistry and radiopharmaceutical product labeling. Int J Rad Appl Instrum B, Nucl Med Biol. 1986;13(2):83–8.
89. Rossouw DD, Macheli L. Large-scale synthesis of no-carrier-added [123I]mIBG, using two different stannylated precursors. J Label Compd Radiopharm. 2009;52:499–503.
90. Shimotake T, Tsuda T, Aoi S, Fumino S, Iwai N. Iodine 123 metaiodobenzylguanidine radio-guided navigation surgery for recurrent medullary thyroid carcinoma in a girl with multiple endocrine neoplasia type 2B. J Pediatr Surg. 2005;40(10):1643–6.
91. Martelli H, Ricard M, Larroquet M, Wioland M, Paraf F, Fabre M, Josset P, Helardot PG, Gauthier F, Terrier-Lacombe MJ, Michon J, Hartmann O, Tabone MD, Patte C, Lumbroso J, Gruner M. Intraoperative localization of neuroblastoma in children with 123I- or 125I-radiolabeled metaiodobenzylguanidine. Surgery. 1998;123(1):51–7.
92. Einspieler I, Novotny A, Okur A, Essler M, Martignoni ME. First experience with image-guided resection of paraganglioma. Clin Nucl Med. 2014; 39(8):e379–81.

93. Ricard M, Tenenbaum F, Schlumberger M, Travagli JP, Lumbroso J, Revillon Y, Parmentier C. Intraoperative detection of pheochromocytoma with iodine-125 labelled meta-iodobenzylguanidine: a feasibility study. Eur J Nucl Med. 1993; 20(5):426–30.
94. Cuntz MC, Levine EA, O'Dorisio TM, Watson JC, Wray DA, Espenan GD, McKnight C, Meier JR, Weber LJ, Mera R, O'Dorisio MS, Woltering EA. Intraoperative gamma detection of 125I-lanreotide in women with primary breast cancer. Ann Surg Oncol. 1999;6(4):367–72.
95. Woltering EA, Barrie R, O'Dorisio TM, O'Dorisio MS, Nance R, Cook DM. Detection of occult gastrinomas with iodine 125-labeled lanreotide and intraoperative gamma detection. Surgery. 1994; 116(6):1139–46; discussion 1146–37.
96. Schirmer WJ, O'Dorisio TM, Schirmer TP, Mojzisik CM, Hinkle GH, Martin Jr EW. Intraoperative localization of neuroendocrine tumors with 125I-TYR(3)-octreotide and a hand-held gamma-detecting probe. Surgery. 1993;114(4):745–51; discussion 751–42.
97. Dawson PM, Blair SD, Begent RH, Kelly AM, Boxer GM, Theodorou NA. The value of radioimmunoguided surgery in first and second look laparotomy for colorectal cancer. Dis Colon Rectum. 1991; 34(3):217–22.
98. Gu J, Zhao J, Li Z, Yang Z, Zhang J, Gao Z, Wang Y, Xu G. Clinical application of radioimmunoguided surgery in colorectal cancer using 125I-labeled carcinoembryonic antigen-specific monoclonal antibody submucosally. Dis Colon Rectum. 2003; 46(12):1659–66.
99. Percivale P, Bertoglio S, Meszaros P, Canavese G, Cafiero F, Gipponi M, Campora E, Gasco M, Badellino F. Radioimmunoguided surgery after primary treatment of locally advanced breast cancer. J Clin Oncol. 1996;14(5):1599–603.
100. Percivale P, Bertoglio S, Meszaros P, Schenone F, Gipponi M, Moresco L, Cosso M, Badellino F. Radioimmunoguided surgery with different iodine-125 radiolabeled monoclonal antibodies in recurrent colorectal cancer. Semin Surg Oncol. 1998;15(4): 231–4.
101. Martin Jr EW, Tuttle SE, Rousseau M, Mojzisik CM, O'Dwyer PJ, Hinkle GH, Miller EA, Goodwin RA, Oredipe OA, Barth RF, et al. Radioimmunoguided surgery: intraoperative use of monoclonal antibody 17-1A in colorectal cancer. Hybridoma. 1986;5 Suppl 1:S97–108.
102. Nieroda CA, Mojzisik C, Hinkle G, Thurston MO, Martin Jr EW. Radioimmunoguided surgery (RIGS) in recurrent colorectal cancer. Cancer Detect Prev. 1991;15(3):225–9.
103. O'Dwyer PJ, Mojzisik CM, Hinkle GH, Rousseau M, Olsen J, Tuttle SE, Barth RF, Thurston MO, McCabe DP, Farrar WB, et al. Intraoperative probe-directed immunodetection using a monoclonal antibody. Arch Surg. 1986;121(12):1391–4.
104. Wang C, Wang Y, Su X, Lin B, Xu X, Zhang M, Li J, Xu G. [Iodine-125 labeled monoclonal antibody 3H11: in radioimmunoguided surgery for primary gastric cancer]. Zhonghua Wai Ke Za Zhi [Chinese Journal of Surgery]. 2000;38(7):507–9.
105. Gray RJ, Giuliano R, Dauway EL, Cox CE, Reintgen DS. Radioguidance for nonpalpable primary lesions and sentinel lymph node(s). Am J Surg. 2001;182(4): 404–6.
106. van Riet YE, Maaskant AJ, Creemers GJ, van Warmerdam LJ, Jansen FH, van de Velde CJ, Rutten HJ, Nieuwenhuijzen GA. Identification of residual breast tumour localization after neo-adjuvant chemotherapy using a radioactive 125 Iodine seed. Eur J Surg Oncol. 2010;36(2):164–9.
107. Alderliesten T, Loo CE, Pengel KE, Rutgers EJ, Gilhuijs KG, Vrancken Peeters MJ. Radioactive seed localization of breast lesions: an adequate localization method without seed migration. Breast J. 2011;17(6):594–601.
108. Donker M, Drukker CA, Valdes Olmos RA, Rutgers EJ, Loo CE, Sonke GS, Wesseling J, Alderliesten T, Vrancken Peeters MJ. Guiding breast-conserving surgery in patients after neoadjuvant systemic therapy for breast cancer: a comparison of radioactive seed localization with the ROLL technique. Ann Surg Oncol. 2013;20(8):2569–75.
109. Hughes JH, Mason MC, Gray RJ, McLaughlin SA, Degnim AC, Fulmer JT, Pockaj BA, Karstaedt PJ, Roarke MC. A multi-site validation trial of radioactive seed localization as an alternative to wire localization. Breast J. 2008;14(2):153–7.
110. Moore GE. Use of radioactive diiodofluorescein in the diagnosis and localization of brain tumors. Science. 1948;107:569–71.
111. Ashkenazy M, Davis L, Martin J. An evaluation of the technic and results of the radioactive di-iodofluorescein test for the localization of intracranial lesions. J Neurosurg. 1951;8(3):300–14.
112. Moore GE. Fluorescein as an agent in the differentiation of normal and malignant tissues. Science. 1947;106(2745):130–1.
113. Morris Jr AC, Barclay TR, Tanida R, Nemcek JV. A miniaturized probe for detecting radioactivity at thyroid surgery. Phys Med Biol. 1971;16(3):397–404.
114. Scurry WC, Lamarre E, Stack B. Radioguided neck dissection in recurrent metastatic papillary thyroid carcinoma. Am J Otolaryngol. 2006;27(1):61–3.
115. Rubello D, Salvatori M, Ardito G, Mariani G, Al-Nahhas A, Gross MD, Muzzio PC, Pelizzo MR. Iodine-131 radio-guided surgery in differentiated thyroid cancer: outcome on 31 patients and review of the literature. Biomed Pharmacother. 2007;61(8):477–81.
116. Fasshauer H, Freundlieb O, Dostal G, Littmann K, Tharandt L, Strotges MW. Intraoperative localization of pheochromocytoma metastases using 131I-metabenzylguanidine. Nuklearmedizin. 1984;23(4):203–5.
117. Aitken DR, Hinkle GH, Thurston MO, Tuttle SE, Martin DT, Olsen J, Haagensen Jr DE, Houchens D, Martin Jr EW. A gamma-detecting probe for

radioimmune detection of CEA-producing tumors. Successful experimental use and clinical case report. Dis Colon Rectum. 1984;27(5):279–82.
118. Xu G, Zhang M, Liu B, Li Z, Lin B, Xu X, Jin M, Li J, Wu J, Dong Z. Radioimmunoguided surgery in gastric cancer using 131-I labeled monoclonal antibody 3H11. Semin Surg Oncol. 1994;10:88–94.
119. Sanchez-Crespo A, Andreo P, Larsson SA. Positron flight in human tissues and its influence on PET image spatial resolution. Eur J Nucl Med Mol Imaging. 2004;31(1):44–51.
120. Zervos EE, Desai DC, DePalatis LR, Soble D, Martin Jr EW. 18F-labeled fluorodeoxyglucose positron emission tomography-guided surgery for recurrent colorectal cancer: a feasibility study. J Surg Res. 2001;97(1):9–13.
121. Jacobson O, Kiesewetter DO, Chen X. Fluorine-18 radiochemistry, labeling strategies and synthetic routes. Bioconjug Chem. 2015;26(1):1–18.
122. Laverman P, McBride WJ, Sharkey RM, Eek A, Joosten L, Oyen WJ, Goldenberg DM, Boerman OC. A novel facile method of labeling octreotide with (18)F-fluorine. J Nucl Med. 2010;51(3):454–61.
123. Gulec SA, Hoenie E, Hostetter R, Schwartzentruber D. PET probe-guided surgery: applications and clinical protocol. World J Surg Oncol. 2007;5:65.
124. Vos CG, Hartemink KJ, Muller S, Oosterhuis JW, Meijer S, van den Tol MP, Comans EF. Clinical applications of FDG-probe guided surgery. Acta Chir Belg. 2012;112(6):414–8.
125. Kraeber-Bodere F, Cariou B, Curtet C, Bridji B, Rousseau C, Dravet F, Charbonnel B, Carnaille B, Le Neel JC, Mirallie E. Feasibility and benefit of fluorine 18-fluoro-2-deoxyglucose-guided surgery in the management of radioiodine-negative differentiated thyroid carcinoma metastases. Surgery. 2005;138(6):1176–82; discussion 1182.
126. Wadas TJ, Wong EH, Weisman GR, Anderson CJ. Coordinating radiometals of copper, gallium, indium, yttrium, and zirconium for PET and SPECT imaging of disease. Chem Rev. 2010;110(5):2858–902.
127. Notni J, Pohle K, Wester HJ. Comparative gallium-68 labeling of TRAP-, NOTA-, and DOTA-peptides: practical consequences for the future of gallium-68-PET. EJNMMI Res. 2012;2(1):28.
128. Clark WA, Izotova L, Philipova D, Wu W, Lin L, Pestka S. Site-specific 32P-labeling of cytokines, monoclonal antibodies, and other protein substrates for quantitative assays and therapeutic application. Bio Tech. 2002;Suppl:76–8, 80–77.
129. Randerath K, Randerath E. 32P-postlabeling methods for DNA adduct detection: overview and critical evaluation. Drug Metab Rev. 1994;26(1–2):67–85.
130. Chakravarty R, Pandey U, Manolkar RB, Dash A, Venkatesh M, Pillai MR. Development of an electrochemical 90 Sr-90 Y generator for separation of 90 Y suitable for targeted therapy. Nucl Med Biol. 2008;35(2):245–53.
131. Minarik D, Sjogreen-Gleisner K, Linden O, Wingardh K, Tennvall J, Strand SE, Ljungberg M. 90Y Bremsstrahlung imaging for absorbed-dose assessment in high-dose radioimmunotherapy. J Nucl Med. 2010;51(12):1974–8.
132. Selwyn RG, Nickles RJ, Thomadsen BR, DeWerd LA, Micka JA. A new internal pair production branching ratio of 90Y: the development of a non-destructive assay for 90Y and 90Sr. Appl Radiat Isot. 2007;65(3):318–27.
133. Lhommel R, Goffette P, Van den Eynde M, Jamar F, Pauwels S, Bilbao JI, Walrand S. Yttrium-90 TOF PET scan demonstrates high-resolution biodistribution after liver SIRT. Eur J Nucl Med Mol Imaging. 2009;36(10):1696.
134. Moore GE, Peyton WT, et al. The clinical use of sodium fluorescein and radioactive diiodofluorescein in the localization of tumors of the central nervous system. Minn Med. 1948;31(10):1073–6.
135. Cundiff JD, Wang YZ, Espenan G, Maloney T, Camp A, Lazarus L, Stolier A, Brooks R, Torrance B, Stafford S, O'Leary JP, Woltering EA. A phase I/II trial of 125I methylene blue for one-stage sentinel lymph node biopsy. Ann Surg. 2007;245(2):290–6.
136. van der Poel HG, Buckle T, Brouwer OR, Valdes Olmos RA, van Leeuwen FWB. Intraoperative laparoscopic fluorescence guidance to the sentinel lymph node in prostate cancer patients: clinical proof of concept of an integrated functional imaging approach using a multimodal tracer. Eur Urol. 2011;60:826–33.
137. Spinelli AE, Ferdeghini M, Cavedon C, Zivelonghi E, Calandrino R, Fenzi A, Sbarbati A, Boschi F. First human Cerenkography. J Biomed Opt. 2013;18(2):20502.
138. Chin PTK, Beekman CAC, Buckle T, Josephson L, van Leeuwen FWB. Multispectral visualization of surgical safety-margins using fluorescent marker seeds. Am J Nucl Med Mol Imaging. 2012;2(2):151–62.
139. Hu H, Cao X, Kang F, Wang M, Lin Y, Liu M, Li S, Yao L, Liang J, Liang J, Nie Y, Chen X, Wang J, Wu K. Feasibility study of novel endoscopic Cerenkov luminescence imaging system in detecting and quantifying gastrointestinal disease: first human results. Eur Radiol. 2015;25(6):1814–22.
140. Mitchell GS, Gill RK, Boucher DL, Li C, Cherry SR. In vivo Cerenkov luminescence imaging: a new tool for molecular imaging. Philos Trans A Math Phys Eng Sci. 2011;369(1955):4605–19.
141. Blower PJ, Kettle AG, O'Doherty MJ, Collins RE, Coakley AJ. 123I-methylene blue: an unsatisfactory parathyroid imaging agent. Nucl Med Commun. 1992;13(7):522–7.
142. Link EM, Blower PJ, Costa DC, Lane DM, Lui D, Brown RS, Ell PJ, Spittle MF. Early detection of melanoma metastases with radioiodinated methylene blue. Eur J Nucl Med. 1998;25(9):1322–9.
143. Harkrider WW, Diebold AE, Maloney T, Espenan G, Wang YZ, Stafford SJ, Camp A, Frey D, Chappuis C,

Woltering EA. An extended phase II trial of iodine-125 methylene blue for sentinel lymph node identification in women with breast cancer. J Am Coll Surg. 2013;216(4):599–605; discussion 605–596.
144. Chu M, Wan Y. Sentinel lymph node mapping using near-infrared fluorescent methylene blue. J Biosci Bioeng. 2009;107(4):455–9.
145. Brouwer OR, Buckle T, Vermeeren L, Klop WM, Balm AJ, van der Poel HG, van Rhijn BW, Horenblas S, Nieweg OE, van Leeuwen FW, Valdes Olmos RA. Comparing the hybrid fluorescent-radioactive tracer indocyanine green-99mTc-nanocolloid with 99mTc-nanocolloid for sentinel node identification: a validation study using lymphoscintigraphy and SPECT/CT. J Nucl Med. 2012;53(7):1034–40.
146. Brouwer OR, van den Berg NS, Matheron HM, van der Poel HG, van Rhijn BW, Bex A, van Tinteren H, Valdes Olmos RA, van Leeuwen FW, Horenblas S. A hybrid radioactive and fluorescent tracer for sentinel node biopsy in penile carcinoma as a potential replacement for blue dye. Eur Urol. 2014;65(3):600–9.
147. KleinJan GH, van den Berg NS, Brouwer OR, de Jong J, Acar C, Wit EM, Vegt E, van der Noort V, Valdes Olmos RA, van Leeuwen FW, van der Poel HG. Optimisation of fluorescence guidance during robot-assisted laparoscopic sentinel node biopsy for prostate cancer. Eur Urol. 2014;66(6):991–8.
148. van den Berg NS, Brouwer OR, Schaafsma BE, Matheron HM, Klop WM, Balm AJ, van Tinteren H, Nieweg OE, van Leeuwen FW, Valdes Olmos RA. Multimodal surgical guidance during sentinel node biopsy for melanoma: combined gamma tracing and fluorescence imaging of the sentinel node through use of the hybrid tracer indocyanine green-tc-nanocolloid. Radiology. 2015;275(2):521–9.
149. Thorek DL, Riedl CC, Grimm J. Clinical Cerenkov luminescence imaging of (18)F-FDG. J Nucl Med. 2014;55(1):95–8.
150. Farwell MD, Pryma DA, Mankoff DA. PET/CT imaging in cancer: current applications and future directions. Cancer. 2014;120(22):3433–45.
151. Maurer AH, Elsinga P, Fanti S, Nguyen B, Oyen WJ, Weber WA. Imaging the folate receptor on cancer cells with 99mTc-etarfolatide: properties, clinical use, and future potential of folate receptor imaging. J Nucl Med. 2014;55(5):701–4.
152. van de Watering FC, Rijpkema M, Perk L, Brinkmann U, Oyen WJ, Boerman OC. Zirconium-89 labeled antibodies: a new tool for molecular imaging in cancer patients. Biomed Res Int. 2014;2014:203601.
153. Azhdarinia A, Ghosh P, Ghosh S, Wilganowski N, Sevick-Muraca EM. Dual-labeling strategies for nuclear and fluorescence molecular imaging: a review and analysis. Mol Imaging Biol. 2012;14(3):261–76.
154. Kuil J, Buckle T, van Leeuwen FWB. Imaging agents for the chemokine receptor 4 (CXCR4). Chem Soc Rev. 2012;41(15):5239–61.
155. Seibold U, Wangler B, Schirrmacher R, Wangler C. Bimodal imaging probes for combined PET and OI: recent developments and future directions for hybrid agent development. Biomed Res Int. 2014;2014:153741.
156. Bunschoten A, Buckle T, Visser N, Kuil J, Yuan H, Josephson L, Vahrmeijer AL, van Leeuwen FWB. Multimodal interventional molecular imaging of tumor margins and distant metastases by targeting the αvβ3 integrin. Chembiochem. 2012;13(7):1039–45.
157. Thorp-Greenwood FL, Coogan MP. Multimodal radio- (PET/SPECT) and fluorescence imaging agents based on metallo-radioisotopes: current applications and prospects for development of new agents. Dalton Trans. 2011;40(23):6129–43.
158. Kuil J, Velders AH, van Leeuwen FWB. Multimodal tumor-targeting peptides functionalized with both a radio- and a fluorescent label. Bioconjug Chem. 2010;21(10):1709–19.